Fluid Phase Equilibria 566 (2023) 113635

Contents lists available at ScienceDirect

Fluid Phase Equilibria

journal homepage: www.sciencedirect.com/journal/fluid-phase-equilibria

Perspective article

A predictive group-contribution framework for the thermodynamic modelling of CO_2 absorption in cyclic amines, alkyl polyamines, alkanolamines and phase-change amines: New data and SAFT-γ Mie parameters

Felipe A. Perdomo [a], Siti H. Khalit [a,1], Edward J. Graham [a], Fragkiskos Tzirakis [b], Athanasios I. Papadopoulos [b], Ioannis Tsivintzelis [b,c], Panos Seferlis [b,d], Claire S. Adjiman [a], George Jackson [a], Amparo Galindo [a,*]

[a] Department of Chemical Engineering, Sargent Centre for Process Systems Engineering, Institute for Molecular Science and Engineering, Imperial College London, South Kensington Campus, London SW7 2AZ, United Kingdom
[b] Chemical Process and Energy Resources Institute, Centre for Research and Technology Hellas, 57001 Thermi, Thessaloniki, Greece
[c] Department of Chemical Engineering, Aristotle University of Thessaloniki, 54124, Thessaloniki, Greece
[d] Department of Mechanical Engineering, Aristotle University of Thessaloniki, PO Box 454, 54124, Thessaloniki, Greece

ARTICLE INFO

Keywords:
SAFT-γ Mie
CO_2 capture
Amine
Phase-change solvent
Group contribution

ABSTRACT

A significant effort is under way to identify improved solvents for carbon dioxide (CO_2) capture by chemisorption. We develop a predictive framework that is applicable to aqueous solvent + CO_2 mixtures containing cyclic amines, alkyl polyamines, and alkanolamines. A number of the mixtures studied exhibit liquid–liquid phase separation, a behaviour that has shown promise in reducing the energetic cost of CO_2 capture. The proposed framework is based on the SAFT-γ Mie group-contribution (GC) approach, in which chemical reactions are described via physical association models that allow a simpler, implicit, treatment of the chemical speciation characteristic of these mixtures. We use previously optimized group interaction parameters between some amine groups and water (Perdomo et al., 2021), and develop new group interactions for the cNH, cN, NH_2, NH, N, cCHNH, and cCHN groups with CO_2; a set of second-order group parameters are also developed to account for proximity effects in some alkanolamines. A combination of literature data and new experimental measurements for the absorption of CO_2 in aqueous cyclohexylamine systems obtained in our current work, are used to develop and test the proposed models. The SAFT-γ Mie GC approach is used to predict the thermodynamics of selected mixtures, including ternary phase diagrams and mixing properties relevant in the context of CO_2 capture. The current work constitutes a substantial extension of the range of aqueous amine-based solvents that can be modelled and thus offers the most comprehensive thermodynamically consistent platform to date to screen novel candidate solvents for CO_2 capture.

1. Introduction

Reducing human emissions of greenhouse gases is a critical environmental concern, which has motivated extensive research on pollutant-gas capture in the search for more effective technologies. Among the most accepted short-term strategies in this context is the capture and storage of carbon dioxide CO_2 (CCS) [1]. Currently the use of aqueous solutions of amines is the preferred option for reducing CO_2 emissions from fossil fuel combustion. Industrially, the most commonly-used solvents for CO_2 chemisorption are based on aqueous solutions of alkanolamines, such as monoethanolamine (MEA), diethanolamine (DEA), N-methyldiethanolamine (MDEA), and 2-amino-2-methyl-1-propanol (AMP). These solvents exhibit a high reactivity with CO_2, leading to the formation of stable carbonates, but the high energetic cost of solvent recovery, the propensity of these solvents to undergo degradation, their corrosiveness and the environmental and health impacts resulting from degradation and solvent losses remain important drawbacks to overcome [7]. There is therefore an urgent

* Corresponding author.
E-mail address: a.galindo@imperial.ac.uk (A. Galindo).
[1] Current address: PETRONAS Research Sdn Bhd, Kuala Lumpur 43000, Malaysia.

https://doi.org/10.1016/j.fluid.2022.113635
Received 5 June 2022; Received in revised form 10 October 2022; Accepted 13 October 2022
Available online 19 October 2022

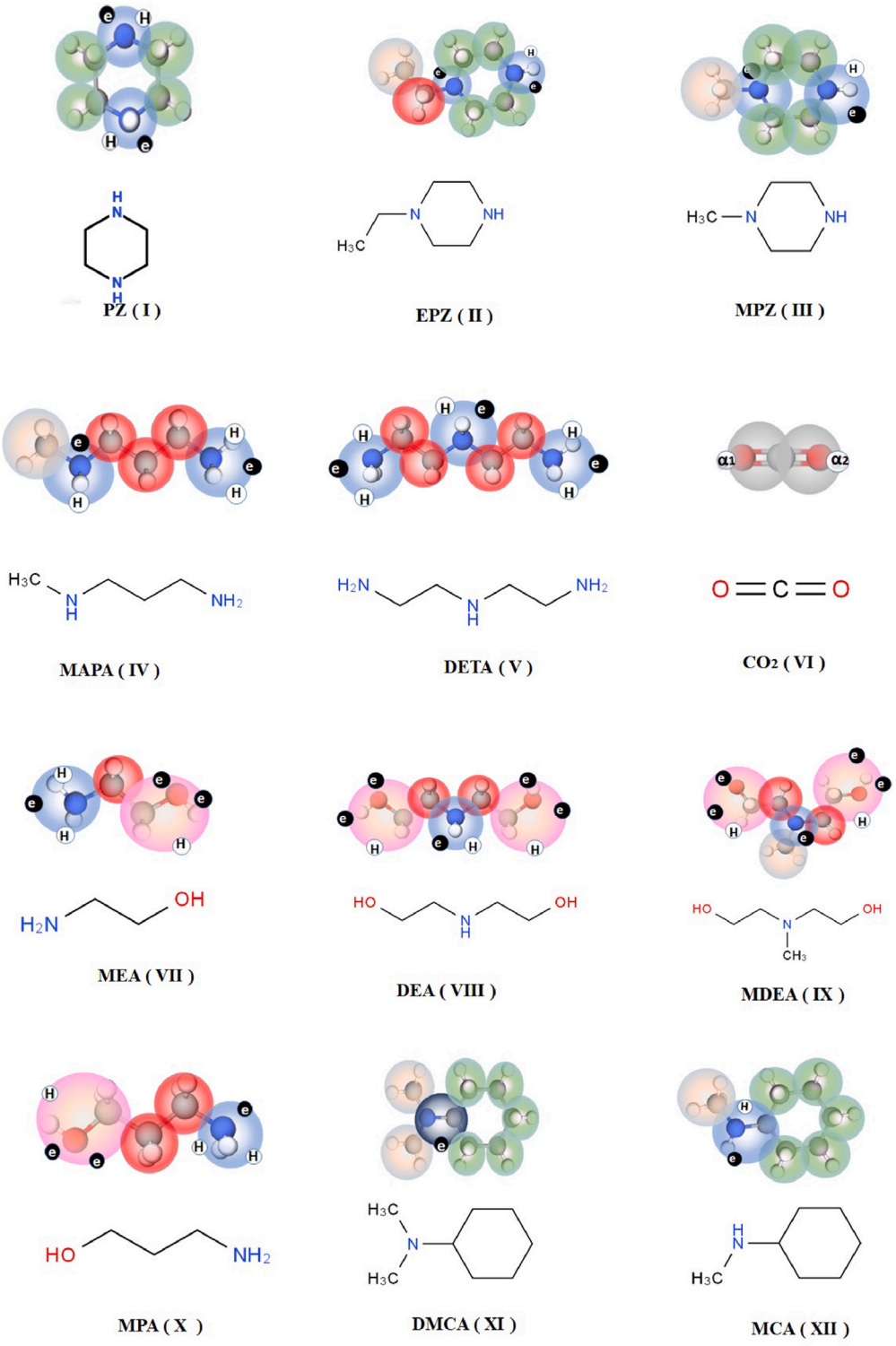

Fig. 1. Representative cyclic, alkyl, and alkanolamines, and carbon dioxide alongside their corresponding SAFT-γ Mie models: (I) piperazine (PZ); (II) *N*-ethylpiperazine (EPZ); (III) *N*-methylpiperazine (MPZ); (IV) *N*-Methyl-1,3-propanediamine (MAPA); (V) Diethylenetriamine (DETA); (VI) carbon dioxide (CO_2); (VII) monoethanolamine (MEA); (VIII) diethanolamine (DEA); (IX) *N*-Methyldiethanolamine (MDEA); (X) 3-amino-1-propanol (MPA); (XI) *N*-methylcyclohexylamine (MCA); and (XII) *N*,*N*-dimethylcyclohexylamine (DMCA).

need to develop novel solvents that allow one to overcome these issues and are suitable for the large-scale deployment of post-combustion capture (PCC) processes. Alternative solvents should thus exhibit desirable properties such as high thermal and chemical stability as well as high mass transfer and cyclic capacity, and a low cost of regeneration.

A number of aqueous solvent systems have been proposed in order to meet the aforementioned criteria. Among solvents that exhibit high CO_2 solubility and resistance to degradation, aqueous solutions of a wide range of cyclic amines have been studied in the search for improved mass transfer and absorption capacity. For instance, cyclic

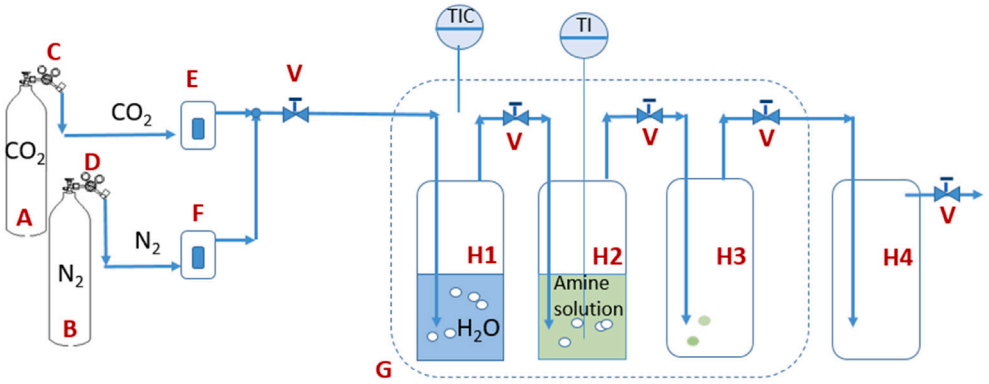

Fig. 2. A simplified scheme of the experimental apparatus. A: CO_2 tank; B: N_2 tank; C and D: Pressure regulators; E: CO_2 Mass flow controller; F: N_2 Mass flow controller; H1–H4: Gas wash bottles (250 mL); G: Thermostated bath; V: valves.
Source: Reproduced from Tzirakis et al. [2] with permission from Elsevier.

diamines such as piperazine (PZ) have been investigated extensively as they exhibit faster mass transfer than alkanolamines [21–23], as well as a higher resistance to thermal degradation. Cyclic amines have also been considered as a good alternative to overcome the high volatility of traditional solvents that results in amine losses and emissions [24]. As far as operational cyclic capacity and regeneration duty are concerned, Li et al. [10] investigated potential solvent candidates taken from a set piperazine-based amines and their mixtures, suggesting that blends composed of MPZ and PZ are the most promising, delivering good affordability when the cyclic capacity is accounted for in the overall cost of the process.

Amongst other approaches and technologies aimed at enhancing performance, those based upon the modification of the physico-chemical properties of the solvent are of special relevance to our current work. In particular Kossmann et al. [25] studied the effect of adding water-immiscible organic compounds (e.g., *n*-hexane and *n*-octane) to aqueous solutions of MEA in order to reduce the energy requirements for regeneration. They demonstrated that the boiling temperature of the reboiler can be lowered significantly due to the presence of a miscibility gap at the desorber conditions. Following their study, amine-based solvents with tunable phase behaviour have been considered as promising alternatives to improve the energy efficiency of post-combustion carbon capture [26–28].

In the CO_2 absorption literature, aqueous solutions of amines (pure or mixed) that exhibit demixing of the liquid phase are known as phase-change solvents (PCSs). PCSs present liquid–liquid demixing when loaded with CO_2 and/or when the temperature is changed, forming one CO_2-lean liquid phase and one CO_2-enriched liquid phase. The use of these biphasic solvents has important advantages for absorption–desorption CO_2 capture processes, as the CO_2-lean phase can be sent back to the absorber without regeneration, such that only the CO_2-enriched phase needs to be sent to the stripping section. Several advantages are expected as a result: the overall energy requirements for solvent recovery are reduced, a lower temperature is needed for solvent regeneration, and there is a larger driving force to absorb CO_2 due to a lower overall concentration of CO_2 in the recycled solvent. These features translate into a more efficient CO_2 capture process [26–31].

A wide range of potential PCSs with varying molecular structures, including linear, branched aliphatic, and cyclic amines, are currently being considered in order to test their suitability for PCC processes. Zhang et al. [31] investigated the fluid-phase behaviour, absorption–desorption performance, and thermal degradation of selected biphasic cyclohexylamines, such as *N*,*N*- dimethylcyclohexylamine (DMCA) and *N*-methylcyclohexylamine (MCA), and their blends with *N*-methyl-diethanolamine (MDEA) and 2-amino-2-methyl-1-propanol (AMP).
They found that TBS-3, a ternary mixture with a specific composition of DMCA + MCA + AMP, met all the criteria to be considered a desirable PCS (low phase-change temperature, high net CO_2 loading, and remarkable chemical stability). By blending aqueous mixtures of diethylethanolamine (DEEA) with 3-(methylamino)propylamine (MAPA), Pinto et al. [29] found that, upon CO_2 loading, some of the amine mixtures (e.g., a blend of 5M DEEA and 2M MAPA) separated into two liquid phases. This biphasic solvent was found to exhibit a high CO_2 absorption and cyclic capacity, and to regenerate at lower temperatures than those used in the traditional MEA-based process. Liu et al. [27] later put forward two biphasic solvents comprising binary mixtures of DEEA + MEA and of DEEA + 2-((2-aminoethyl)amino) ethanol (AEEA), both exhibiting higher absorption loading and desorption capacity than MEA. These findings highlight the delicate balance that exists between molecular structure and solvent performance, and the importance of developing a good understanding of the link between the macroscopic CO_2 absorption and the specific molecular interactions within CO_2 + amine + water mixtures to design effective novel solvents.

In view of the wide range of amine molecular structures that are potentially suitable for CO_2 capture and of the high cost and time requirements of experimental screening efforts, it is highly desirable to develop predictive approaches to aid in the selection of the promising candidates to be explored, thereby reducing the experimental effort. As numerous combinations of potential solvent candidates can be proposed (i.e., aqueous solutions of pure amines, blends of amines, or amines + organic compounds) there is a need for the integrated consideration of numerous property-based criteria to guide the identification of solvents with high CO_2 capture potential. From a thermodynamic point of view, however, the study of the properties of mixtures involved in CO_2 chemisorption and of the underlying phenomena is very challenging.

In aqueous solution amine groups tend to interact strongly with surrounding water molecules through hydrogen bonds, giving rise to complex hydration structures [32,33] that crucially affect the solubility of the amine (or blend) in water. The combination of the formation of hydrogen bonds and the hydrophobic nature of the alkyl groups can also lead to the demixing of the liquid phase, often bound by a lower critical solution temperature (LCST) [34]; the mixtures are fully miscible at temperatures below the LCST, but present two liquid phases above this point. At higher temperatures heterogeneous azeotropes may appear, which increase the complexity of the fluid-phase behaviour.

A further challenge arises when CO_2 is dissolved in the aqueous amine solution, as the mixture undergoes a complex set of chemical (speciation) reactions that lead to the formation of ionic species [35–37]. CO_2 reacts with water to form carbonic acid, with the hydroxide ion to form bicarbonate, and with amines to form carbamates. When the solvent contains tertiary amines, these promote the hydration of CO_2 to produce a greater amount of bicarbonate [38]. In solvents that exhibit partial miscibility, such as in PCSs, depending on the temperature, pressure, CO_2 loading and solvent concentration, the ionic species that

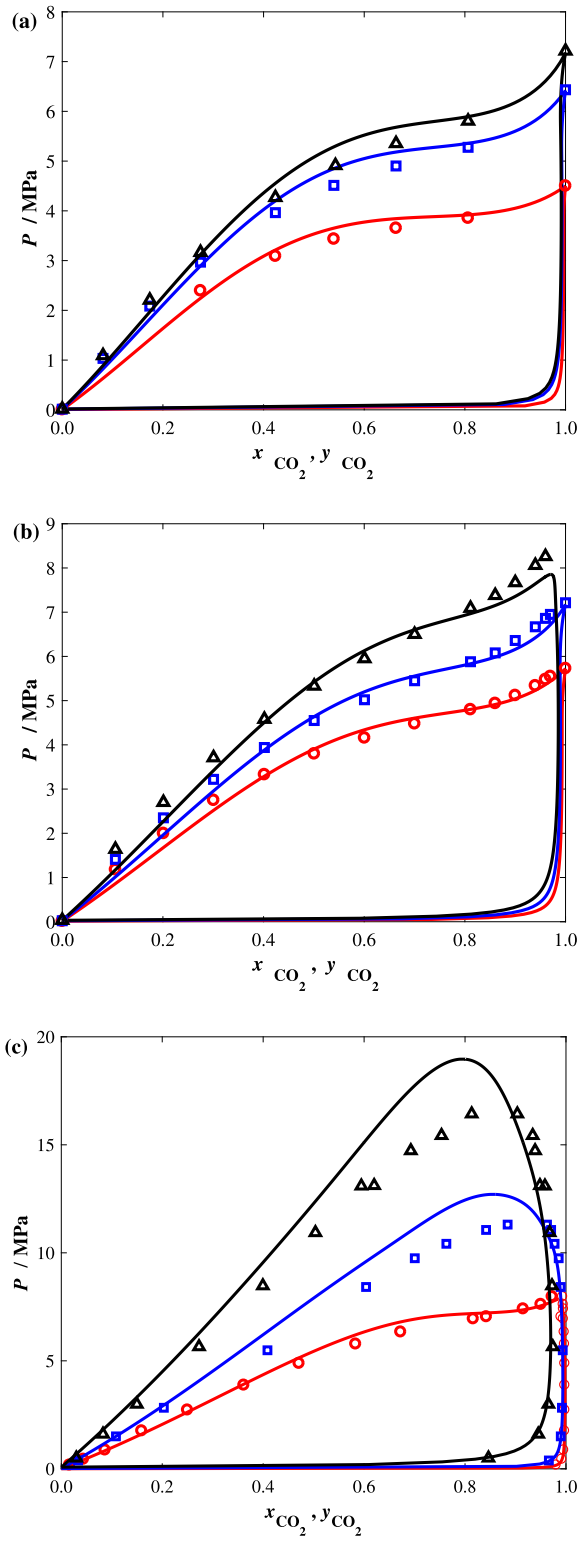

Fig. 3. Isothermal pressure-composition slices of the vapour–liquid equilibria of binary mixtures of: (a) cyclohexane + CO_2 [3,4] at T = 283.15 K (circles), 298.15 K (squares), and 303.15 K (triangles); (b) methylcyclopentane + CO_2 [4,5] at T = 293.15 K (circles), 303.15 K (squares), and 313.15 K (triangles); (c) ethylcyclohexane + CO_2 [6] at T = 310.93 K (circles), 338.71 K (squares) and 394.43 K (triangles). The symbols correspond to experimental data and the continuous curves to calculations using the SAFT-γ Mie group-contribution approach.

result from the absorption of CO_2 will distribute either in one or in both of the liquid phases [39]. At higher temperatures, the two liquid phases which contain a range of ionic species are in equilibrium with a

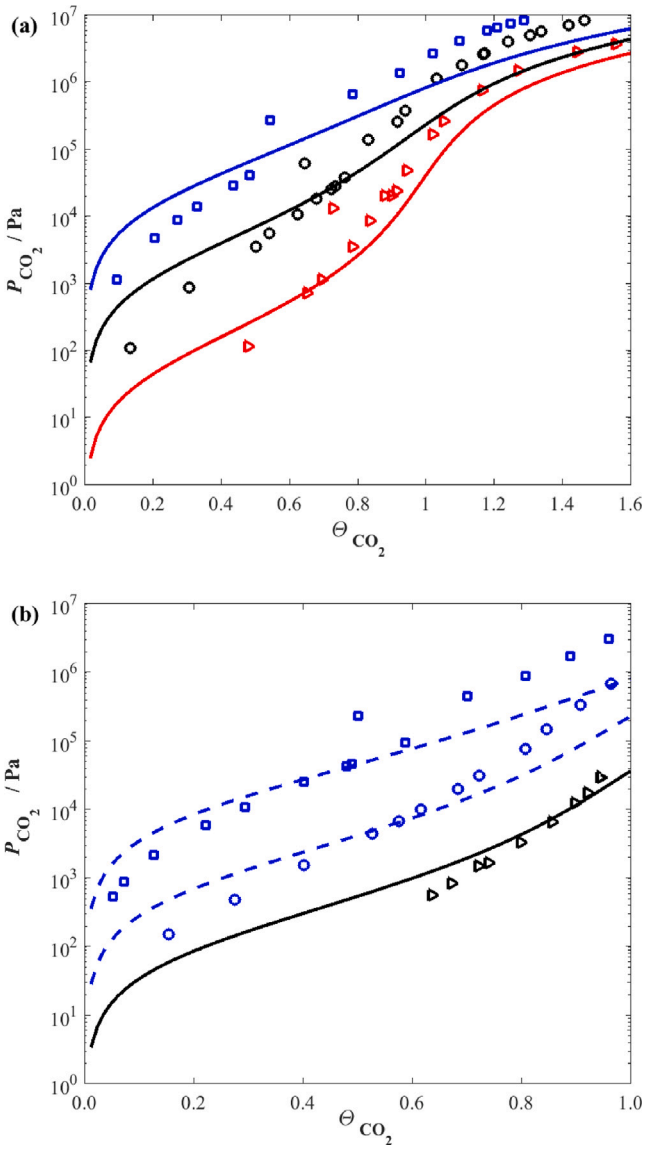

Fig. 4. Isotherms of the vapour–liquid equilibrium of PZ + H_2O + CO_2 mixtures shown as partial pressure of CO_2 as a function of the CO_2 loading, Θ_{CO_2}: (a) PZ concentration of 2.0297 molal (15w_{PZ}%) at T = 313.15 K (red triangles), 353.15 K (black circles), 393.15 K (blue squares); (b) PZ concentration of 0.9890 molal (8w_{PZ}%) at 313.15 K (black triangles) and of 4.0440 molal (26w_{PZ}%]) at 353.15 K (blue circles) and 393.15 K (blue squares). The symbols correspond to the experimental data [8], and the continuous and dotted curves to calculations and predictions, respectively, using the SAFT-γ Mie group-contribution approach.

third vapour phase that comprises only molecular species (CO_2, water, amine). Accounting for the impact of these chemical reactions and determining the phase equilibria of these mixtures is a demanding task, requiring not only a detailed molecular model that captures a wide range of intermolecular interactions and provides a careful thermodynamic formulation of the equilibrium and stability conditions, but also a suitable approach to overcome the resulting numerical complexity.

Numerous semi-empirical and theoretical approaches have been used to study the fluid-phase behaviour of CO_2 with aqueous solutions of amines. In most approaches the chemical (equilibrium) reactions in the liquid phase are treated explicitly, with the distribution of molecular and ionic species obtained based on measured chemical equilibrium constants. The solution of the chemical and phase-equilibria equations is carried out using activity coefficient models to treat the deviations from classical behaviour that occur in the liquid phase,

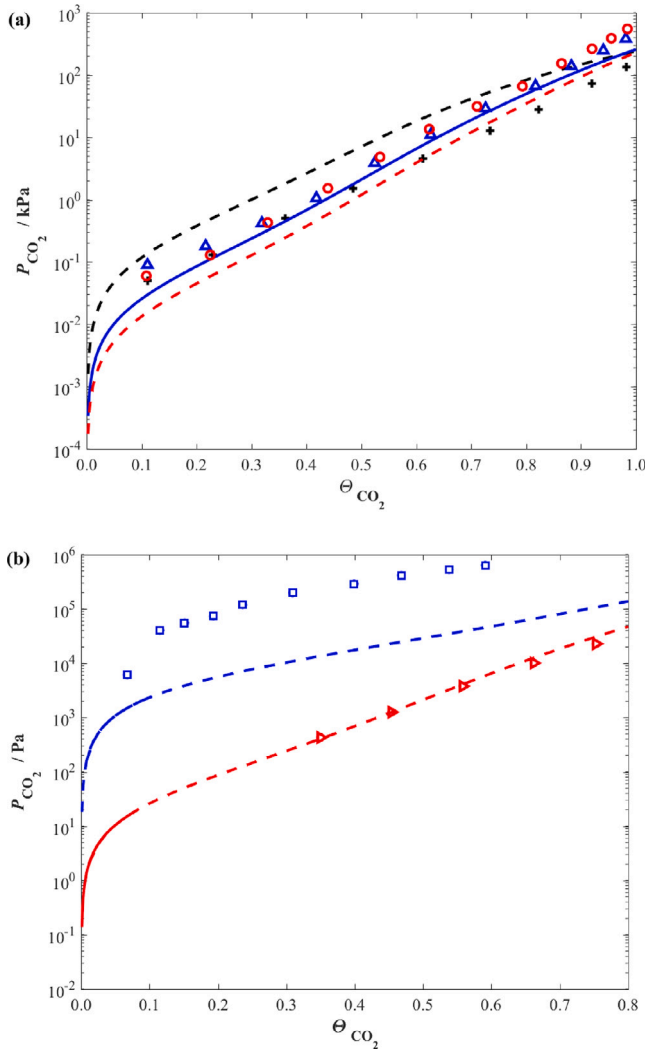

Fig. 5. Isotherms shown as the partial pressure of CO_2 as a function of the CO_2 loading for the vapour–liquid equilibrium of: (a) *N*-methylpiperazine (MPZ) + H_2O + CO_2 at T = 313.15 K and concentrations of $10w_{MPZ}$% (black crosses [9]), $30w_{MPZ}$% (blue triangles [9]), and $40w_{MPZ}$% (red circles citeli2) (black circles); (b) $30w_{EPZ}$% *N*-ethylpiperazine (EPZ) + H_2O + CO_2 at T = 313.15 K (red triangles [10]) and T= 393.15 K (blue squares [10]). The symbols correspond to experimental data, and the continuous and dotted curves to calculations and predictions, respectively, using the SAFT-γ Mie group-contribution approach.

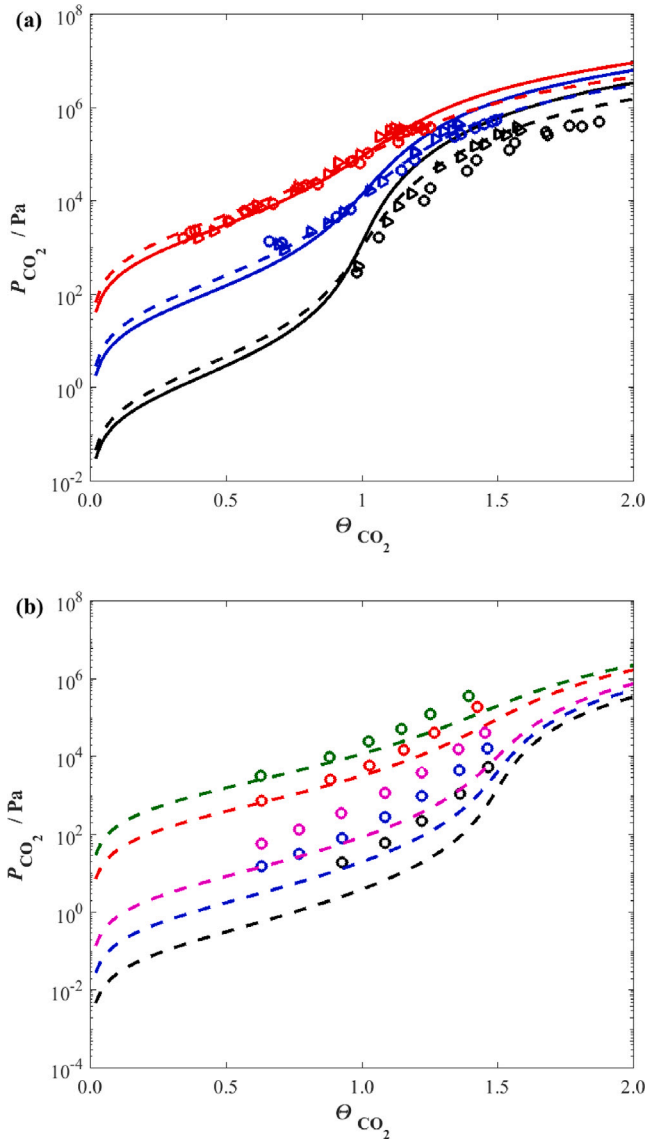

Fig. 6. Isotherms shown as the partial pressure of CO_2 as a function of the CO_2 loading for the vapour–liquid equilibrium of: (a) 3-(methylamino)propylamine (MAPA) + H_2O + CO_2 at T= 313.15 K, 1M (black circles [11] and continuous black curve), T= 313.15 K, 2M (black triangles [11] and dotted black curve), T=353.15 K, 1M (blue circles and continuous blue curve), T=353.15 K, 2M (blue triangles [11], and dotted blue curve), T = 393.15 K, 1M (red circles [11], and continuous red curve), and T = 393.15 K, 2M (red triangles [11], and dotted red curve). The symbols correspond to experimental data and the continuous (1M) and dotted (2M) curves to calculations and predictions, respectively, using the SAFT-γ Mie group-contribution approach. (b) 17 w_{DETA}% N-(2-aminoethyl)-1,2-ethanediamine (DETA) + H_2O + CO_2 at T = 298.15 K (black circles [12]), T= 313.15 K (blue circles [12]), T= 328.15 K (magenta circles [12]), T= 353.15 K (red circles [12]), and T= 373.15 K (green circles [12]). All dotted curves correspond to predictions using the SAFT-γ Mie group-contribution approach.

and fugacities computed from an equation of state (EOS) to account for non-ideal behaviour in the vapour phase [8,40–42]. One of the most widely-used activity coefficient models to describe the physical interactions of amines in aqueous solutions containing ionic species is Pitzer's model [43]. Bougie and Iliuta [40], Ermatchkov et al. [8], and Kamps et al. [44] have studied the absorption of CO_2 in aqueous solutions of piperazine (PZ) by calculating the activity coefficients for all the PZ-derived species with a virial equation of state to represent the fugacities of molecular compounds in the vapour phase. Using Pitzer's parameters obtained from NMR measurements of the concentration of the amine, bicarbonate, carbamate, and CO_2, along with vapour–liquid equilibria data, Böttinger et al. [45,46] modelled the absorption of CO_2 in aqueous solutions of MEA, DEA, *N*-methyldiethanolamine (MDEA), and of MDEA + piperazine (PZ), and thus calculated the distribution profiles of ionic and molecular species in the liquid phase as well as the CO_2 solubility. The approach enables one to correlate the experimental data and results in a good description of the properties of the system within the range of measured temperatures and CO_2 loadings, but requires the introduction of a large number of state-dependent empirical parameters, as well as the availability of an extensive set of experimental data.

The extended universal quasichemical (UNIQUAC) [47] model has also been implemented in this context, not only to consider the effect of the speciation reactions in homogeneous CO_2 chemisorption using conventional alkanolamines (i.e., *N*-methyldiethanolamine) [41], but also to predict the liquid-phase split in PCSs [48,49], An important contribution of this work was to demonstrate that the amount of water in the liquid phase plays a critical role in promoting the hydration of

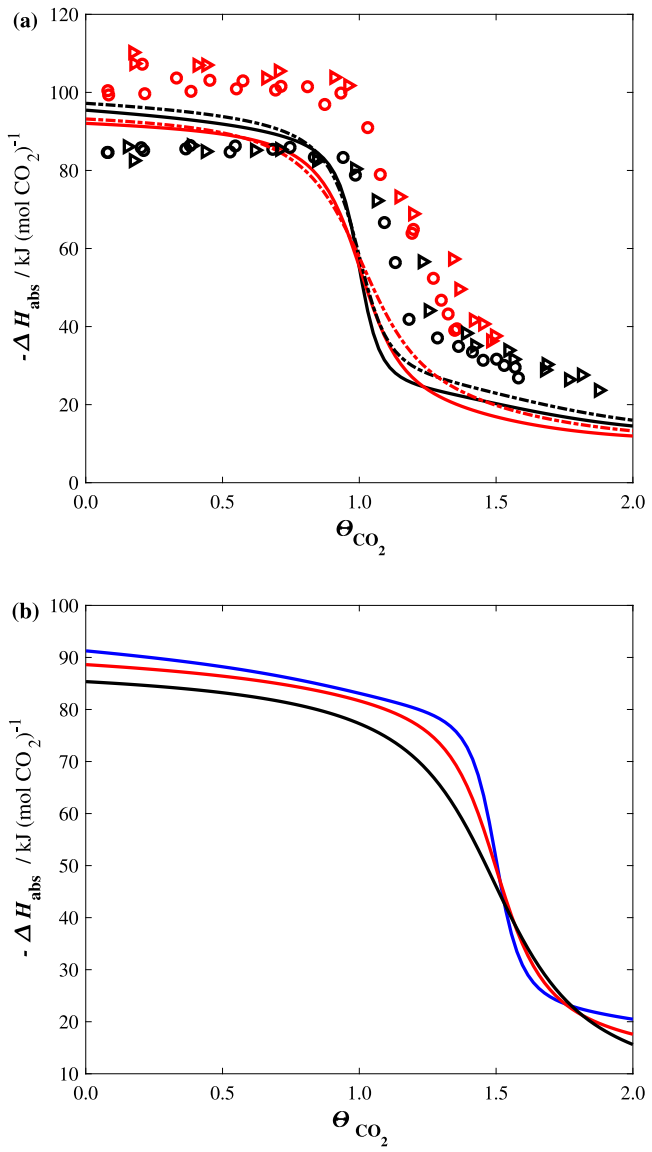

Fig. 7. Differential heat of absorption of CO_2 in aqueous solutions of (a) MAPA at 1 M and T= 313.15 K (black circles [13] and continuous black curve); 1M and T= 353.15 K (red circles [13] and continuous red curve); 2M and T=313.15 K (black triangles [13] and black dotted curve); and 2M and T= 353.15 K (red triangles [13] and red dotted curve). The symbols correspond to experimental data and the curves to predictions using the SAFT-γ Mie group-contribution approach. (b) $20w_{DETA}$% at T= 313.15 K (blue curve), T= 353.15 K (red curve), and T=393.15 K (black curve). All curves represent predictions using the SAFT-γ Mie group-contribution approach.

CO_2 and hence determining the distribution of ionic species. Although this approach requires fewer parameters than Pitzer's model, it is based on the limiting law of Debye–Hückel, and therefore the effects of charged species in the model are represented through the ionic strength alone.

More rigorous and thermodynamically consistent formulations of the activity coefficients have also been used to describe the fluid-phase behaviour and speciation arising from CO_2 absorption in aqueous solutions of amines. For instance, the refined electrolyte-nonrandom two liquid (e-NRTL) model [50] has been used to predict the solubility of CO_2 in aqueous solutions of alkanolamines such as MEA and MDEA [42]. In this approach the inconsistency in the reference state used in the calculation of the long-range interactions (infinite dilution in a continuum) and that used to account for the effect of the short-range interactions (infinitely diluted aqueous solution) were corrected by incorporating a Born term [51,52] for the excess free energy of solvation.

A different approach involves the direct implementation of an equation of state (EOS) to model all fluid phases. This has the advantage of accounting for pressure effects and avoiding the selection of different standard reference states for the different phases. Moreover, in order to account explicitly for the set of chemical reactions in EOS models, the composition profile of both the molecular and ionic species can be expressed as a function of density, temperature, and the corresponding equilibrium constant. Fürst and Renon [61] developed an expression for the residual Helmholtz free energy that includes non-ionic and ionic contributions. The approach was used to calculate the solubility of CO_2 and other acid gases (e.g., H_2S) in aqueous solutions of diethanolamine (DEA) [62], *N*-methyldiethanolamine (MDEA) [63], and cyclic amines (e.g., piperazine) [64]. The method delivers a very good representation of CO_2 solubility and of the equilibrium pressure as a function of temperature and solvent concentration. It relies, however, on the availability of extensive experimental information on the equilibrium constants of the chemical reactions.

Taking advantage of the fact that the chemical identity of the reactants (CO_2 and amines) does not change drastically during the CO_2 absorption process, it is also possible to employ physical approaches to account for the formation of new species (i.e., carbamate and carbonate) in the system, thus bypassing the need for equilibrium constant data. It has been shown that physical approaches based on perturbation theories such as the statistical associating fluid theory (SAFT) [71–73], lead to a description that is equivalent to that obtained with either chemical or quasi-chemical theories for mixtures of species that form hydrogen bonds [74]. In chemical approaches, an equation of state is combined with a chemical-equilibrium scheme [75] to represent the formation of new species and aggregates. On the other hand, in physical approaches, the formation of aggregates and new species is represented with a molecular model of association that forms an integral part of the underlying equation of state. The free energy of an associating (or reacting) fluid is thus obtained from an intermolecular potential model that incorporates a number of associating (or reacting) sites that mediate the formation of aggregates (or complexes).

A key advantage of the physical approach is that the nature of the chemical reactions present in the system does not need to be specified *a priori* and consequently there is no need to provide equilibrium constants. This has allowed the development of an implicit treatment of the speciation reactions relevant to CO_2 capture [77–79]. For example, using the statistical association fluid theory for potentials of variable range (SAFT-VR) [80,81], with square well (SW) potentials, Rodríguez et al. [78] predicted the degree of speciation of the mixture of MEA + CO_2 + H_2O by incorporating two acceptor sites placed on CO_2 to mimic the formation of tightly bonded aggregates that represent the main ionic species (carbamate, bicarbonate) in solution. The model allowed for accurate predictions of the mole fraction of carbamate and bicarbonate in aqueous solutions of MEA without the need for experimentally measured equilibrium constants.

Building on these findings, SAFT group contribution (GC) approaches such as the SAFT-γ SW [82,83] and SAFT-γ Mie [84–86] EOSs have also been used to model aqueous solutions of alkanolamines and CO_2 [79, 87]. In these methods, a heteronuclear model is implemented, and the group-contribution premise that the properties of a molecule can be determined from the contributions of the chemical functional groups (moieties) in the system is adopted. The advantage of GC approaches is that the thermodynamic behaviour of mixtures including solvents that have not been synthesized or tested can be predicted, provided the relevant group parameters are available. In our previous work we have shown that the use of the SAFT-γ Mie GC EOS provides accurate models of a wide range of amines, including linear, branched, and cyclic amines, and their mixtures with water [87]. The parameters describing the functional groups and their interactions were determined in a sequential manner, such that the influence of the surrounding alkyl

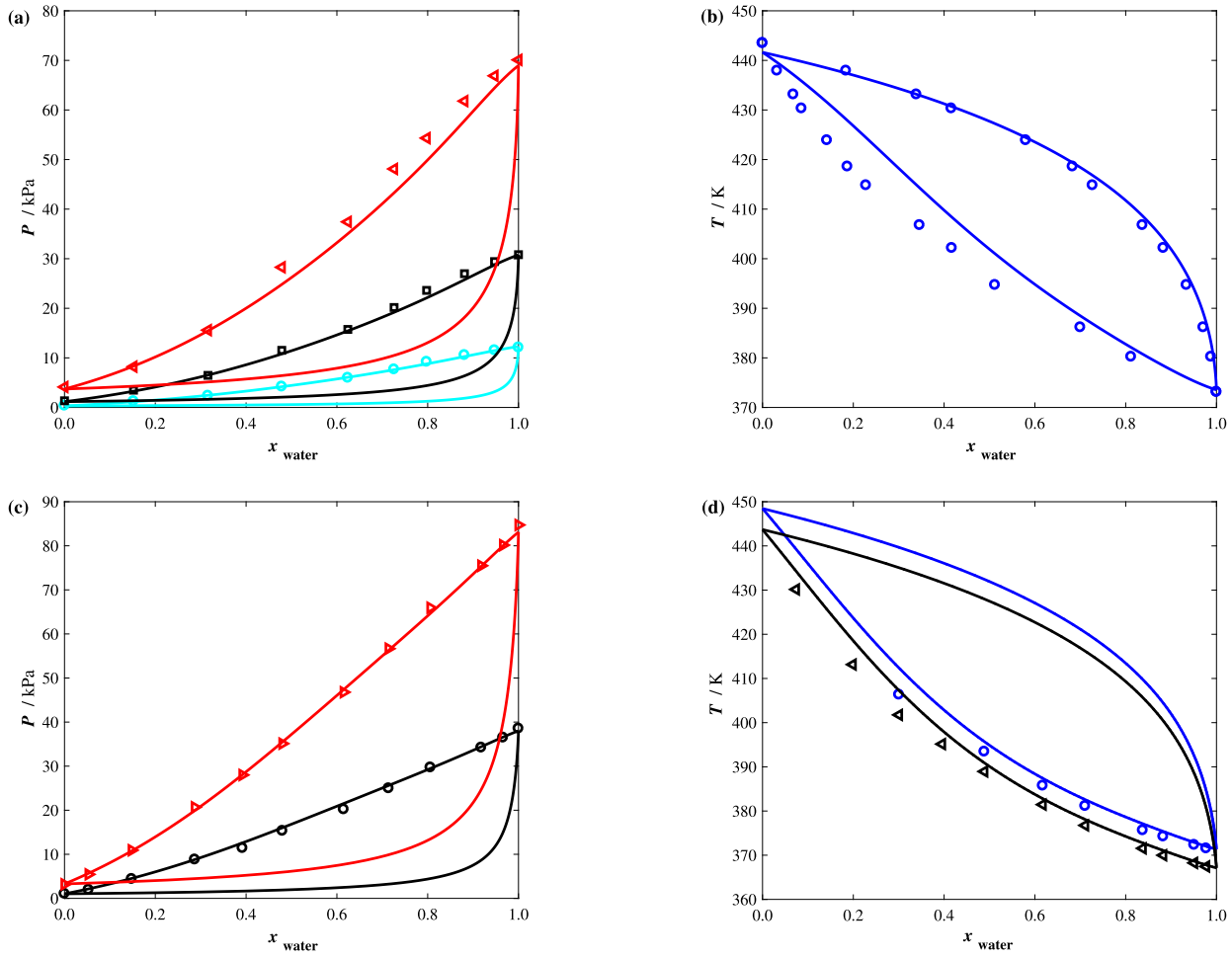

Fig. 8. Vapour–liquid equilibria of aqueous solutions of monoethanolamine (MEA) at (a) T= 323.15 K (cyan circles [14]), T= 343.15 K (black squares [14]) and T= 363.15 K (red triangles [14]); (b) P = 101.325 kPa (blue circles [15]); and vapour–liquid equilibria of aqueous solutions of monopropanolamine (MPA) at (c) T= 348.15 K (black circles [16]) and T= 368.15 K (red triangles [16]); (d) P = 93.3 kPa (blue circles [16]) and P = 79.993 kPa (black triangles [16]). The continuous curves represent calculations using the SAFT-γ Mie group-contribution approach, and the symbols correspond to the experimental data.

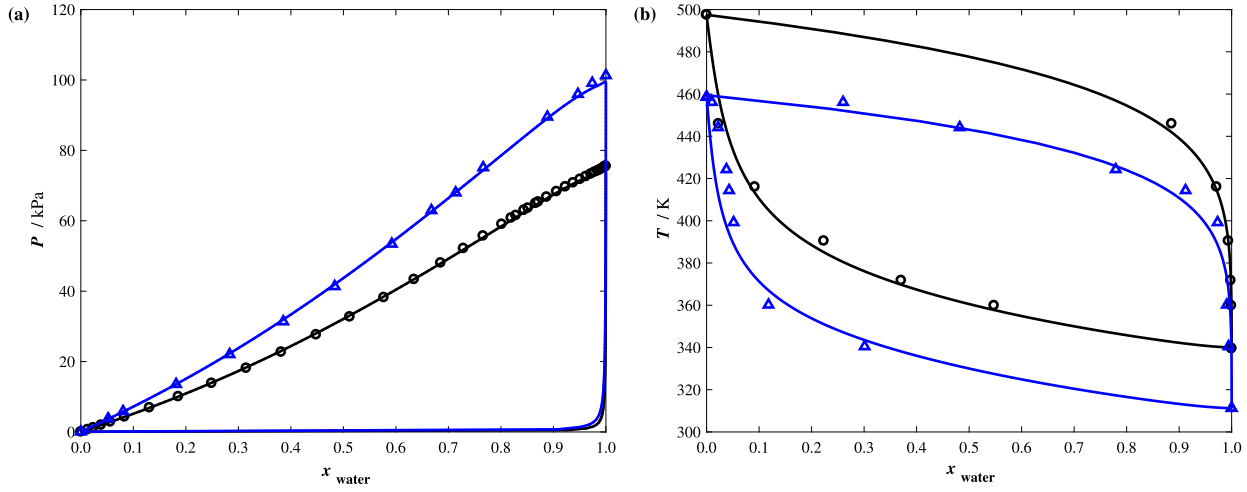

Fig. 9. Vapour–liquid equilibria of aqueous solutions of diethanolamine (DEA) at (a) T= 365.15 K (black circles [17]), T= 373.15 K (blue triangles [18]); (b) P = 26.7 kPa (black circles [19], P = 6.65 kPa (blue triangles [20]). The continuous curves represent calculations using the SAFT-γ Mie group-contribution approach, and the symbols correspond to the experimental data.

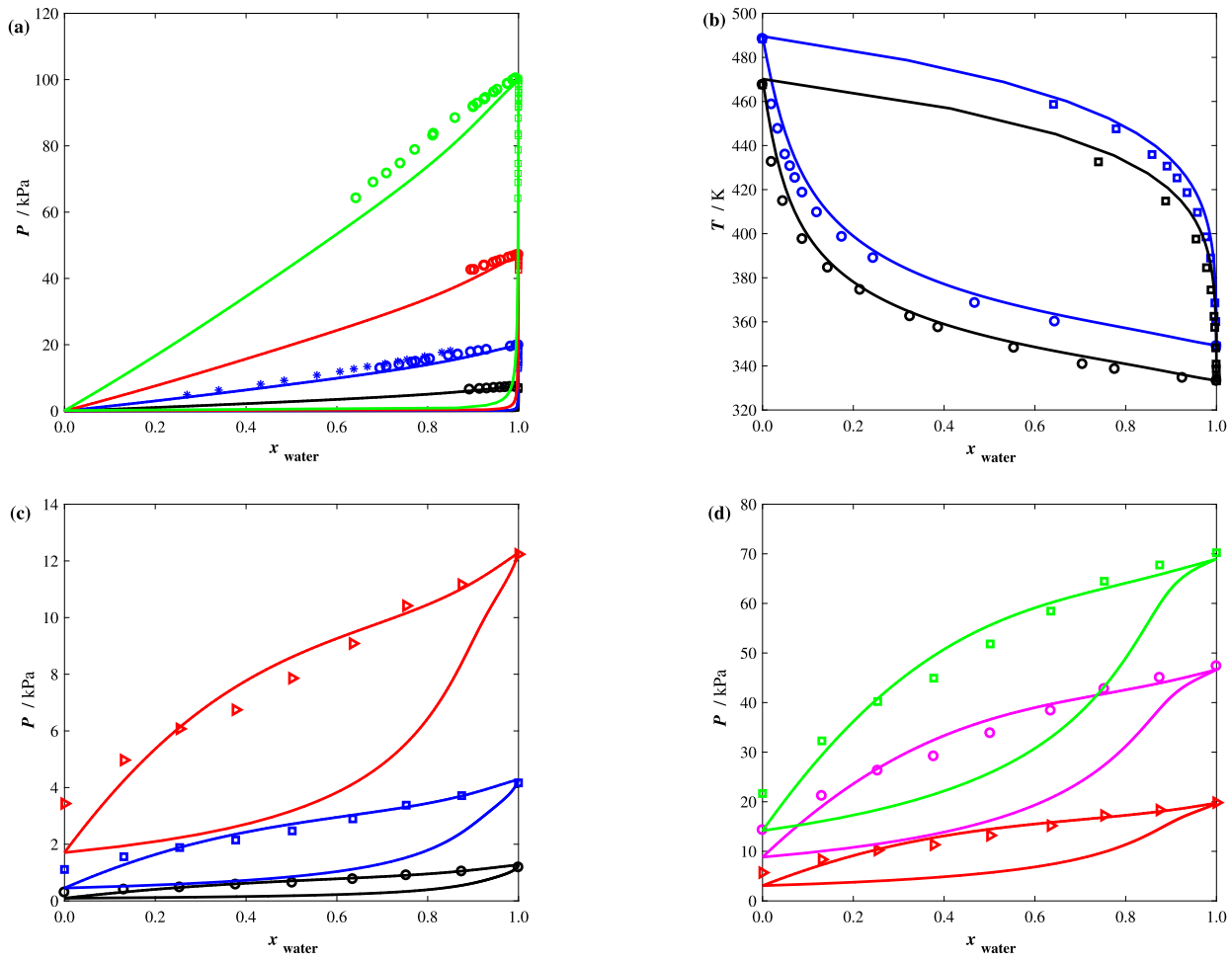

Fig. 10. Vapour–liquid equilibria of aqueous solutions of methyl diethanolamine (MDEA) at (a) T = 313.15 K (black circles [53]), T = 333.15 K (blue circles [53], blue stars [54]), T = 353.15 K (red circles [53]) and T = 373.15 K (green circles [53]); (b) P = 20.0 kPa (black circles and squares [55]) and P = 40.0 kPa (blue circles and squares [55]); and isothermal temperature composition slices (P–x) of the vapour–liquid equilibria of aqueous solutions of N,N-dimethyl monoethanolamine (DMMEA) at (c) T = 283.15 K (black circles [56]), T = 303.15 K (blue squares [56]), and T = 323.15 K (red triangles [56]); (d) T = 333.15 K (red triangles [56]), T = 353.15 K (magenta circles [56]), and T = 363.15 K (green squares [56]). The continuous curves represent calculations using SAFT-γ Mie group-contribution approach, and the symbols correspond to experimental data.

substituents on the ability of nitrogen atoms to participate in hydrogen bonds was captured. The models developed for the various amine chemical groups were shown to be transferable, leading to an accurate representation of the fluid-phase behaviour of a variety of pure amines and of aqueous solutions of amines, even in the presence of lower critical solution temperatures (LCST) and heterogeneous azeotropes. While the development of these models is a necessary step towards the predictive modelling of CO_2 absorption, no reactions were considered nor was CO_2 present in any of the mixtures.

In the current work, we develop predictive group-contribution models for the absorption of CO_2 in a large set of aqueous solutions of amines. New SAFT-γ Mie group interaction parameters are developed to be used for the prediction of the fluid-phase behaviour of the mixtures of interest over broad ranges of temperature, pressure, and composition. This makes it possible to systematically explore and test a range of alternative solvents and to identify promising candidates for CO_2 capture processes. We also carry out experimental measurements of the equilibrium solubility of CO_2 in aqueous solutions of representative biphasic cyclohexylamines (MCA and DMCA), following the procedure described by Tzirakis et al. [2]. Ternary phase diagrams for diverse types of PCS solvents + H_2O + CO_2 systems are predicted in order to study the topology of the fluid-phase diagrams with temperature and pressure. The information obtained from these diagrams is of direct relevance to the search for optimal amine-based solvents for CO_2 capture. It is worth mentioning also that global pressure–temperature (PT) phase diagrams are often useful, although we note that application of the solvents studied in our current work rarely occurs in critical conditions, as separation is not possible in such states. Additionally, the determination of the global phase diagrams is numerically very demanding. As such, PT global phase diagrams are beyond the scope of our current work. In Section 2 the SAFT-γ Mie GC approach and the thermodynamic model used to describe the selected systems are presented, highlighting the implicit treatment of the speciation reactions that take place during the CO_2 absorption. Additionally, we give a summary of the main expressions of the SAFT-γ Mie GC approach. The experimental set-up is presented in Section 3, and the experimental and modelling results are provided in Section 4. Brief conclusions are given in Section 5.

2. Theory and thermodynamic model

2.1. The SAFT-γ Mie equation of state

In the SAFT-γ Mie group-contribution approach [84–86] a heteronuclear model is implemented, with molecules subdivided into distinct functional groups representing the various chemical moieties (see Fig. 1 for a SAFT-γ Mie representation of the molecules of interest here). Each group k is modelled as a fused spherical segment (or v_k^* identical segments). Segments k and l are assumed to interact through Mie

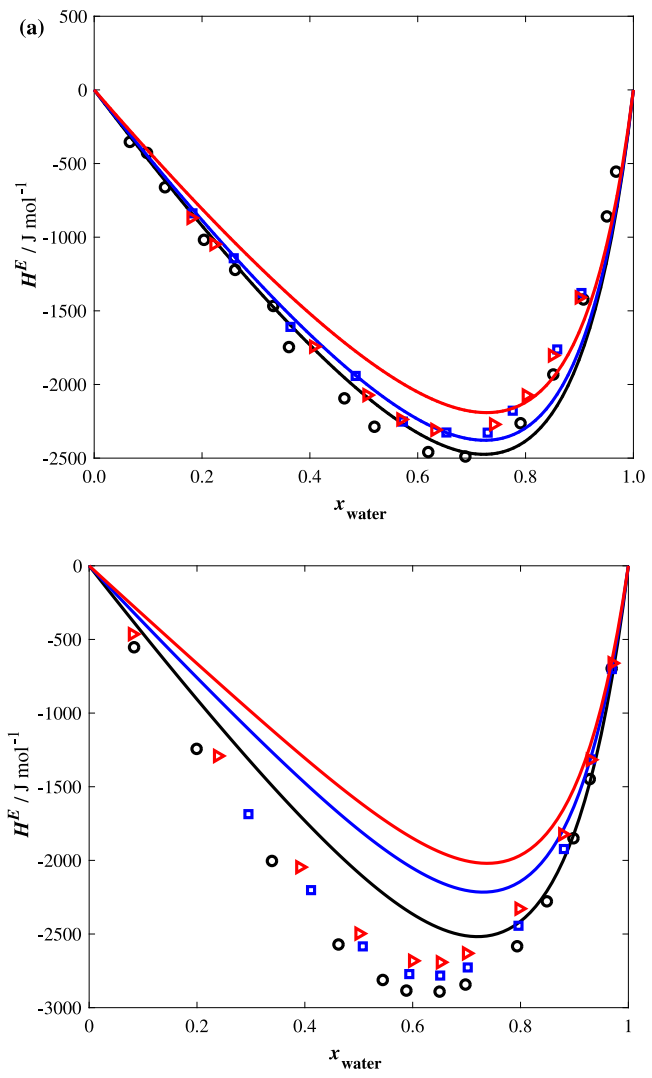

Fig. 11. Isothermal–isobaric excess molar enthalpy of mixing H^E for aqueous solutions of alkanolamines of varying mole fraction x. The symbols represent the experimental data and the continuous curves the predictions with the SAFT-γ Mie group-contribution approach: (a) Methyldiethanol amine + water at $P = 0.1$ MPa and $T = 298.15$ K (black circles [57]), $T = 303.15$ K (blue squares [57]), $T = 313.15$ K (red triangles [57]); (b) N,N–dimethylmonoethanolamine + water at $P = 0.1$ MPa and $T = 298.15$ K (black circles [58]), $T = 313.15$ K (blue squares [58]), $T = 323.15$ K (red triangles [58]).

potentials of variable attractive and repulsive ranges:

$$\Phi_{kl}^{\text{Mie}} = C_{kl}\varepsilon_{kl}\left[\left(\frac{\sigma_{kl}}{r_{kl}}\right)^{\lambda_{kl}^r} - \left(\frac{\sigma_{kl}}{r_{kl}}\right)^{\lambda_{kl}^a}\right], \tag{1}$$

where r_{kl} represents the centre–centre distance between groups k and l, σ_{kl} is the average segment diameter, obtained as the arithmetic mean of the diameters of segments k and l, $-\varepsilon_{kl}$ is the minimum in the potential energy of interaction between segments k and l, and λ_{kl}^r and λ_{kl}^a represent the repulsive and attractive exponents of the inter-segment interactions, respectively. The energy and exponents can either be obtained via appropriate combining rules based on the corresponding parameters for like interactions [84], or can be estimated from experimental data. The prefactor C_{kl} is a function of the exponents and is given by

$$C_{kl} = \frac{\lambda_{kl}^r}{\lambda_{kl}^r - \lambda_{kl}^a}\left(\frac{\lambda_{kl}^r}{\lambda_{kl}^a}\right)^{\frac{\lambda_{kl}^a}{\lambda_{kl}^r - \lambda_{kl}^a}}. \tag{2}$$

Hydrogen bonding is mediated by embedding a set of short-range square-well sites on a segment k. Each site is assigned a type a where $a \in \mathcal{N}_{\text{ST},k}$, the set of site types for group k. The number of site types for group k is defined as $N_{\text{ST},k}$, and there can be multiple sites of each type on a group. The parameters to describe the association between sites of type a on a group k and of type b on a group l include the energy $\varepsilon_{kl,ab}^{\text{HB}}$ and the range (in the form of the bonding volume) $K_{kl,ab}$. In the case of amine groups, two site types, H and e, are typically specified, where e represents the lone pair of electrons on the N atom, and one H site is included per hydrogen atom, with only e–H bonding allowed. For CO_2 molecules, two site types α_1 and α_2, which can interact with amine e sites, are included to mediate the relevant chemical reactions with the amine molecules (note that α_1–α_2 bonding is not permitted).

The total Helmholtz free energy A of a mixture of N_C non-ionic components for a temperature T and volume V is given as the sum of four contributions arising from the perturbation approach:

$$A = A^{\text{IDEAL}} + A^{\text{MONO}} + A^{\text{CHAIN}} + A^{\text{ASSOC}}, \tag{3}$$

where A^{IDEAL} is the ideal free energy of the mixture, A^{MONO} is the residual free energy due to the interactions between monomer Mie segments, A^{CHAIN} is the contribution due to chain formation, and A^{ASSOC} accounts for the contribution to the free energy due to intermolecular association. For a complete description of the theory and full expressions for each of the contributions, we direct the reader to the original SAFT-γ Mie publications [84–86,88].

It is worth describing in detail the contribution to the free energy due to association as it relates to the implicit model of speciation used in our current work. It is given by [89–92]:

$$\frac{A^{\text{ASSOC}}}{N k_B T} = \sum_{i=1}^{N_C} x_i \sum_{k=1}^{N_G} \nu_{k,i} \sum_{a=1}^{N_{\text{ST},k}} n_{k,a}\left[\ln X_{i,k,a} + \frac{1 - X_{i,k,a}}{2}\right] \tag{4}$$

where N is the number of molecules in the mixture, k_B is the Boltzmann constant, N_G is the number of groups in the mixture, x_i, $i = 1, \ldots, N_C$, is the mole fraction of component i, $\nu_{k,i}$ is the number of groups of type k in molecule i, $n_{k,a}$ is the number of sites of type a on group k, and $X_{i,k,a}$ represents the fraction of molecules of component i that are not bonded at a site of type a on group k; it is obtained from the solution of the mass action equation [73].

Of specific interest for our work is $X_{\text{CO}_2,\text{CO}_2,\alpha_s}$, the fraction of CO_2 molecules not bonded at site α_s, with $s = 1, 2$ (note the double CO_2 subscript reflects the fact that CO_2 is a molecule, or component i, and a group k). Sites α_1 and α_2 represent the two acceptor sites of the CO_2 molecular group interacting exclusively with sites of type e on the amine groups. The interaction potential between an e site on an amine group l and an α_s site on CO_2 is modelled as a square well potential with an energy depth of $\varepsilon_{\text{CO}_2,l,\alpha_s,\text{e}}^{\text{HB}}$, and a bonding volume $K_{\text{CO}_2,l,\alpha_s,\text{e}}$. The fraction of CO_2 molecules not bonded at α_s is given by

$$X_{\text{CO}_2,\text{CO}_2,\alpha_s} = \left(1 + \rho \sum_{j=1}^{N_C} x_j \sum_{l \in G_A} \nu_{l,j} n_{l,\text{e}} X_{j,l,\text{e}} \Delta_{\text{CO}_2,j,\text{CO}_2,l,\alpha_s,\text{e}}\right)^{-1} \quad \text{for } s = 1, 2, \tag{5}$$

where G_A is the set of amine groups (G_A = {NH_2, NH, N, cNH, cN, cCHNH, cCHN}), ρ is the mixture density, $\Delta_{\text{CO}_2,j,\text{CO}_2,l,\alpha_s,\text{e}}$ represents the association strength between site α_s on CO_2 and site e on the N atom of amine group l ($l \in G_A$) of component j, given by [84–86]:

$$\Delta_{\text{CO}_2,j,\text{CO}_2,l,\alpha_s,\text{e}} = F_{\text{CO}_2,l,\alpha_s,\text{e}} K_{\text{CO}_2,l,\alpha_s,\text{e}} I_{\text{CO}_2,j}, \tag{6}$$

where $F_{\text{CO}_2,l,\alpha_s,\text{e}} = \left[\exp\left(\varepsilon_{\text{CO}_2,l,\alpha_s,\text{e}}^{\text{HB}}/(k_B T)\right) - 1\right]$ is the Mayer function and $I_{\text{CO}_2,j}$ is a polynomial temperature–density correlation for the association integral for a Lenard-Jones monomer [85,86].

2.2. Speciation and phase equilibria

When carbon dioxide dissolves in aqueous amine solutions, it reacts with water to form bicarbonate (HCO_3^-) and with the amine molecules to form a range of ionic species. In the case of secondary and primary amines, the most prominent route involves the formation of a zwitterionic form of carbamate followed by a proton exchange reaction to form

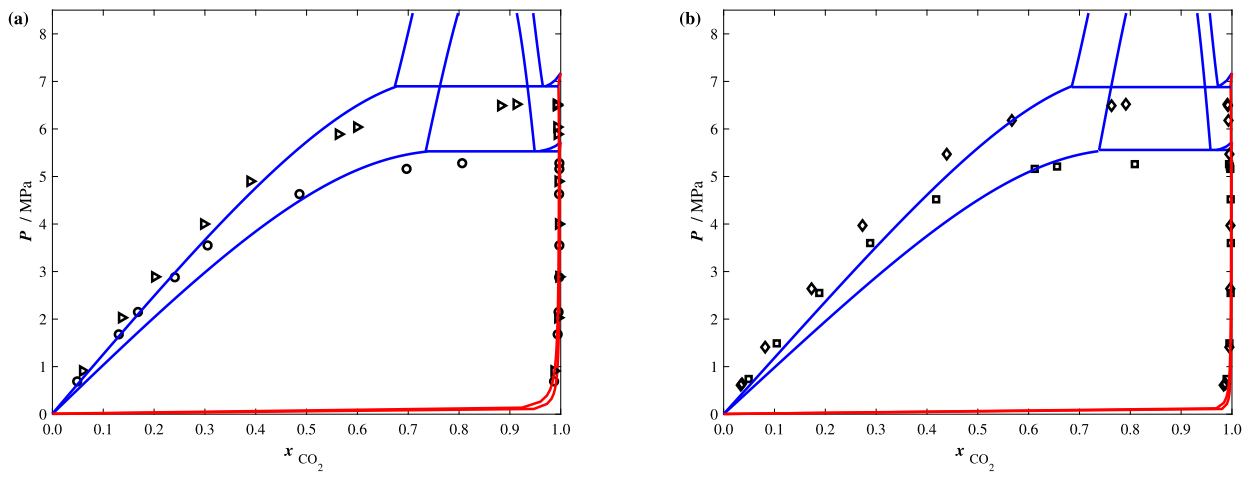

Fig. 12. Isothermal pressure-composition ($P-x$) slices of the vapour–liquid equilibria for (a) ethanol + carbon dioxide at $T = 293.15$ K (circles [59]) and 303.15 K (triangles [59]) and for (b) propanol + carbon dioxide mixture at $T = 293.15$ K (squares [60]) and 303.15 K (diamonds [60]). The symbols correspond to experimental data, and the continuous curves to calculations with the SAFT-γ Mie group-contribution approach.

the respective amine carbamate [38]:

$$CO_2 + 2R'RNH \rightleftharpoons \left[R'RNHCOO^- + R'RNH_2^+\right], \tag{7}$$

and

$$R'RNHCOO^- + H_3O^+ \rightleftharpoons \left[R'RNH_2^+ + HCO_3^-\right], \tag{8}$$

where R′ represents either an alkyl-substituent for secondary amines or a hydrogen atom for primary amines. Ternary amines react with CO_2 by an indirect path promoting the hydration of CO_2 to produce bicarbonate as follows:

$$R''R'R\text{-}N + H_2O + CO_2 \rightleftharpoons \left[R''R'R\text{-}NH^+ + HCO_3^-\right]. \tag{9}$$

The speciation reactions described by Eqs. (7)–(9) are characterized by their reversibility, and by the fact that there is little change in the chemical identity of the reactants (CO_2 and amines). In our current work we take advantage of these features to develop an implicit model of the reactions, thus avoiding the need to specify a priory the dependence of the equilibrium constant on the thermodynamic conditions.

In an implicit description it is possible to extract the fraction of molecules (not) bonded at a given association (reactive) site by considering the association free energy of the system (Eqs. (4) and (5)); this type of information can be used to predict the degree of speciation in the system [78,79]. The ion pairs represented with square brackets on the right hand side of Eqs. (7) and (8) are assumed to be neutral species with no net overall charge. The concentration of carbamate can be deduced from the concentration of CO_2 molecules bonded at both α_1 and α_2 sites, while the concentration of bicarbonate can be obtained from the concentration of CO_2 molecules bonded at only one site:

$$\left[R'RNHCOO^-\right] = x_{CO_2}\left(1 - X_{CO_2,CO_2,\alpha_1}\right)\left(1 - X_{CO_2,CO_2,\alpha_2}\right), \tag{10}$$

and

$$\left[HCO_3^-\right] = x_{CO_2}\left(X_{CO_2,CO_2,\alpha_1} + X_{CO_2,CO_2,\alpha_2} - 2\left(X_{CO_2,CO_2,\alpha_1}X_{CO_2,CO_2,\alpha_2}\right)\right). \tag{11}$$

The expressions for the concentration of carbamate and bicarbonate are the result of the conservation of the chemical elements given the fact that, in our model, CO_2 molecules can only bond to amine molecules, i.e., there is no CO_2–CO_2 and CO_2–H_2O association.

In order to calculate the distribution of the molecular species in each of the coexisting phases, the necessary conditions for phase equilibrium [93,94] are solved for a given number of phases or the solution of the phase stability and equilibrium problem is performed with the HELD algorithm [95,96]. This approach, combined with the fact that the nature of the chemical equilibrium present in a given mixture does not need to be specified explicitly, facilitates the modelling of the solvent mixtures.

2.3. Parameter estimation

In order to specify fully the expressions for the Helmholtz free energy presented in Eq. (3) and model the mixtures of interest, a number of like and unlike group interaction parameters need to be characterized. All of the like parameters are determined by solving a least-squares parameter estimation problem, using experimental data for molecules containing the groups of interest, while the unlike parameters are initially determined using combining rules and then estimated from experimental data when necessary. The combining rules are summarized in Appendix A.

An advantage of the heteronuclear model used in our approach is that pure component data are sufficient in some cases to obtain an accurate estimate of the values of these unlike energetic parameters. Whether pure component or mixture data are used, optimized parameters are obtained by minimizing an objective function F_{Obj} comprising the sum of squares of the relative deviations between experimental data and calculated values of relevant properties, such as saturated-vapour pressures, partial pressures of CO_2 in the vapour phase or the composition of loaded solvent. The objective function is given as

$$\min_{\Theta} f_{\text{obj}} = \frac{1}{N^{\text{exp}}}\sum_{s=1}^{N^{\text{S}}}\sum_{p=1}^{N_s^{\text{P}}}\sum_{i=1}^{N_{s,p}^{\text{D}}} w_{s,p,i}\left(\frac{X_{s,p,i}^{\text{exp}} - X_{s,p,i}^{\text{calc}}(\Theta)}{X_{s,p,i}^{\text{exp}}}\right)^2, \tag{12}$$

where Θ is the vector of model parameters, N^{exp} is the total number of experimental points considered in the parameter estimation, N^{S} is the number of systems (pure components and mixtures) used in the estimation, N_s^{P} is the number of types of properties for system s, $N_{s,p}^{\text{D}}$ is the number of experimental data for system s and property p, and $w_{s,p,i}$ is a weight that controls the relative importance of data point i for property p of system s. We consider here the same weight for each point (i.e., $w_{s,p,i} = 1$, for all (s,p,i)). $X_{s,p,i}^{\text{exp}}$ is the i^{th} measured value of property p of system s, and $X_{s,p,i}^{\text{calc}}(\Theta)$ is the corresponding value calculated with SAFT-γ Mie and the parameters Θ. The estimation of the group parameters is carried out using either the parameter estimation facility of the commercial software package gPROMS ModelBuilder 7.0.7 [97] or that in the software package gSAFT Material Modeller (gSAFTmm) version 1.0.0 [98], both of which use the same implementation of the SAFT-γ Mie EOS. In order to assess the quality of the description, the percentage absolute average deviation (%AAD) of a property p for a given system s is determined as follows:

$$\%\text{AAD}[p] = \frac{1}{N_{s,p}^{\text{D}}}\sum_{i=1}^{N_{s,p}^{\text{D}}}\left|\frac{X_{s,p,i}^{\text{exp}} - X_{s,p,i}^{\text{calc}}}{X_{s,p,i}^{\text{exp}}}\right| \times 100. \tag{13}$$

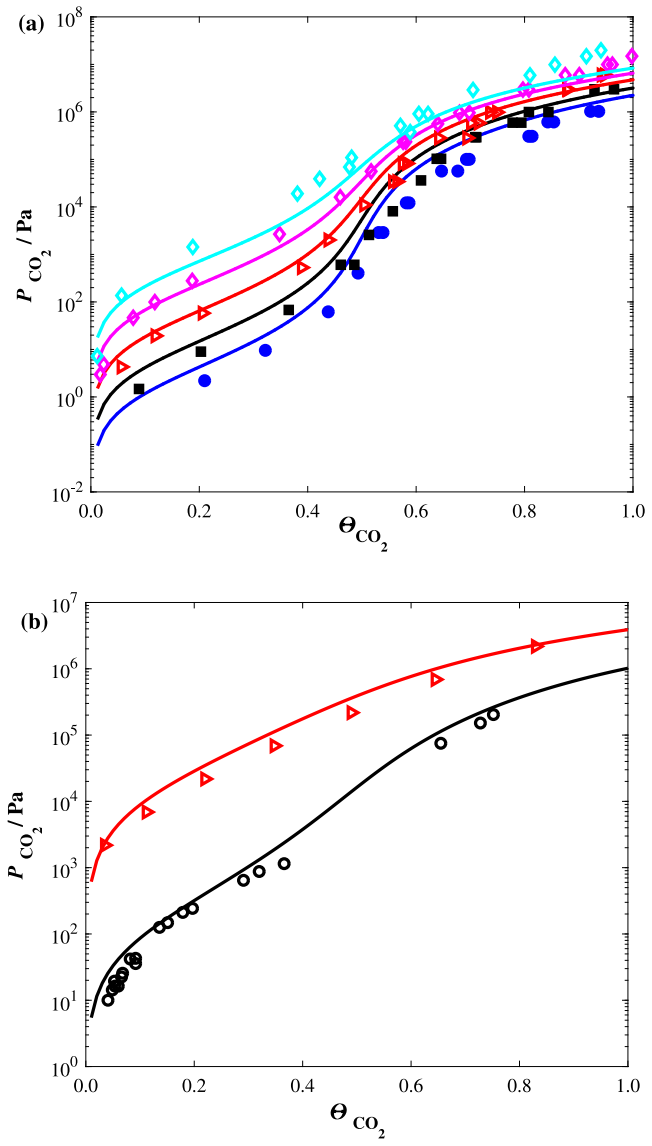

Fig. 13. Isotherms of the vapour–liquid equilibrium of alkanolamines + H_2O + CO_2 in a (a) $30w_{MEA}$% aqueous solution of MEA at T = 298.15 K (blue circles [65]), 313.15 K (black squares [65]), 333.15 K (red triangles [65]), 353.15 K (magenta diamonds [65]), and 373.15 K (cyan diamonds [65]); and (b) $20w_{DEA}$% aqueous solution of DEA at T = 313.15 K (black circles [66]) and 373.15 K (red triangles [66]). The symbols correspond to experimental data and the curves of corresponding colours to calculations with the SAFT-γ Mie group-contribution approach. The filled symbols indicate the experimental data thate are used in the parameter estimation procedure.

The SAFT-γ Mie models for water [88], CO_2 [99], and all of the amine groups [87,100] considered in this work are taken from previous studies. A total of 19 new first- and second-order group interaction parameters are developed in the present study.

3. Experimental measurements

In the case of two of the phase-change solvents considered in our current work (the aqueous solutions of MCA and DMCA), little or no experimental data are available. We carry out new experimental measurements of vapour–liquid and vapour–liquid–liquid equilibria and of CO_2 loading for aqueous solutions of MCA and DMCA, reporting the compositions of the liquid phases in cases where liquid–liquid phase separation is observed. The experimental setup and procedure are described thoroughly in Tzirakis et al. [2] and are therefore only described briefly here.

3.1. Materials

The materials used in the current work are shown in Table 1. All materials were used as received without further purification.

3.2. Experimental apparatus and procedure

The experimental apparatus is presented in Fig. 2. Mixtures of CO_2 and N_2 pass through four gas wash bottles immersed in a thermostated water/oil bath (the variability of temperature during the experiments ranges between 0.8°C at 90°C and 0.1°C at 40°C). The first (H1) gas-wash bottle contains pure water in order to compensate for vaporization losses, the second (H2) contains the aqueous amine solution (approximately 30 mL), while the third (H3), and the fourth (H4, held at lower temperature) are used as traps for potential drifted droplets (not observed in this study) and amine vapours, respectively.

As mentioned by Tzirakis et al. [2], the experimental apparatus compensates, to the extent possible, for water vaporization losses. However, there are also some amine losses due to vaporization, although the amines present relatively high boiling points. Amine losses are an important issue in pilot- (and full-) scale absorbers, such that our experiments can, nevertheless, be considered representative of a pilot-scale absorber. As a result of the amine losses, the experimental procedure results in a reduction of the amine content of the loaded solutions compared to the unloaded (initial) ones. The compositions of both the initial aqueous solution of amine and the CO_2 loaded solution are presented in the following section.

Experiments were performed using CO_2/N_2 gas streams of different composition (the CO_2 partial pressure in the inlet gas stream ranged from 10 to 80 kPa) and gas–liquid contact times of 2–5 h. At the end of each experiment, samples of one or two liquid phases were immediately taken with a calibrated syringe for further analysis. The CO_2 loading was measured using the barium chloride titration method and the total amine content using an acid–base titration technique. In all cases the results were confirmed by GC analysis using a thermal conductivity detector (TCD). All other experimental details can be found in Tzirakis et al. [2].

4. Results

4.1. Parameter tables

The SAFT-γ Mie group-interaction matrix relevant to our current work is presented in Table 2, with the corresponding values for like and unlike group parameters given in Tables 3, 4, 5, 6, and 7. The specific groups used for each of the compounds and mixtures studied are presented in Appendix B. In addition, the workflow we follow for the identification and characterization of new groups, including the determination of second-order interactions is provided in Appendix C.

4.2. CO_2 solubility in aqueous solutions of cyclo- and alkyl-amines

In order to describe the thermodynamic properties of solutions of water + CO_2 + cyclic or linear alkylamines, the unlike interaction parameters between water and the amine groups (NH_2, NH, N, cNH, cN, cCHNH, and cCHN) developed in previous work [87] are adopted here, as are interactions between linear alkyl groups (CH_3 and CH_2) and CO_2 [88]. The interaction parameters between cyclic alkyl groups and CO_2 are developed in this section, using binary mixture phase-equilibrium data. Furthermore, the interaction parameters between

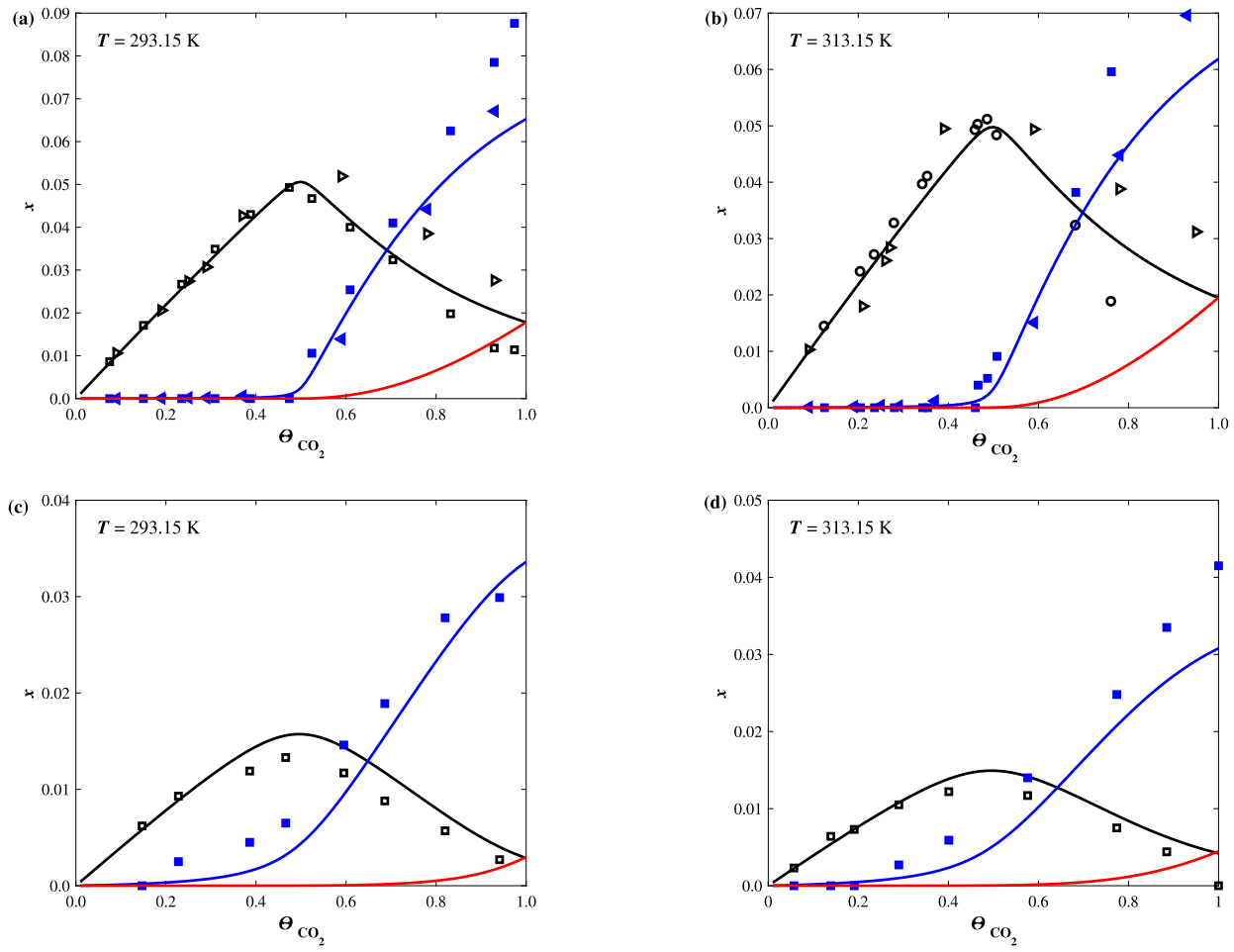

Fig. 14. Predicted mole fraction of carbamate $MEACOO^-$ and bicarbonate HCO_3^- in the liquid phase of a $30w_{MEA}\%$ MEA aqueous solution at (a) $T = 293.15$ K and (b) $T = 313.15$ K at vapour–liquid equilibrium for the ternary mixture of MEA + H_2O + CO_2, as a function of the CO_2 loading, Θ_{CO_2}. The symbols correspond to the experimental data [45,67] with open symbols corresponding to carbamate and filled symbols to bicarbonate. The predicted mole fraction of carbamate $DEACOO^-$ and bicarbonate HCO_3^- in the liquid phase of a 20 $w_{DEA}\%$ DEA aqueous solution at (c) $T = 293.15$ K and (d) $T = 313.15$ K at vapour–liquid equilibrium for the ternary mixture of DEA + H_2O + CO_2 as a function of the CO_2 loading. The symbols correspond to the experimental data [45] with open symbols corresponding to carbamate and filled symbols to bicarbonate. In all cases, the curves correspond to the predictions with the SAFT-γ Mie group-contribution approach.

Table 1
Chemicals used in the current work.

Product name	Abbreviation	CAS-number	Purity	Supplier
Carbon dioxide	CO_2	124-38-9	99.9 (vol%)	Air Liquide
Nitrogen	N_2	7727-37-9	99.9 (vol%)	Air Liquide
Helium	He	7440-59-7	99.99 (vol%)	Air Liquide
N-methyl cyclohexylamine	MCA	100-60-7	99%	Sigma Aldrich
N, *N*-dimethyl cyclohexylamine	DMCA	98-94-2	99%	Sigma Aldrich

CO_2 and amine groups are derived from ternary mixture data of aqueous solutions of alkyl- and cyclo-amines with carbon dioxide, as no binary mixture data involving these groups are available.

4.2.1. Cycloalkane + CO_2 mixtures: cCH–CO_2 and cCH$_2$–CO_2 unlike interaction parameters

Data for the isothermal vapour–liquid equilibria of binary mixtures of cycloalkanes (e.g., cyclohexane and cyclopentane) and monosubstituted cycloalkanes (e.g., methylcyclohexane and methylcyclopentane) with CO_2 are used to estimate the values of the dispersion energies ε_{kl} that best describe the fluid-phase behaviour for the chemical families of compounds comprising the cCH$_2$ and cCH groups with CO_2. The interaction parameters are presented in Table 4.

Fluid-phase diagrams for cyclohexane + CO_2 and methylcyclopentane + CO_2 binary mixtures at different conditions of pressure and temperature are shown in Fig. 3. It is apparent from the figures that the estimated SAFT-γ Mie group parameters lead to an accurate description of the experimental phase behaviour. The suitability of the approach for the description of other mixtures involving the same groups is confirmed by the results presented in Fig. 3(c), where a very good prediction of the isothermal vapour–liquid equilibria for ethylcyclohexane and CO_2 is obtained using the same parameter values.

4.2.2. Cyclic amine + H_2O + CO_2 mixtures: cNH–CO_2 and cN–CO_2 unlike interaction parameters

Isothermal vapour–liquid equilibrium (VLE) data for ternary mixtures of one cyclic amine (piperazine (PZ), methyl piperazine (MPZ), or ethylpiperazine (EPZ)) with water and carbon dioxide are used to estimate the unlike parameters characterizing the interactions of CO_2 with the cyclic secondary and tertiary amine groups (cNH and CN, respectively). In our model, the association interaction between the e site of the nitrogen atom and the reactive α_1 and α_2 sites of CO_2

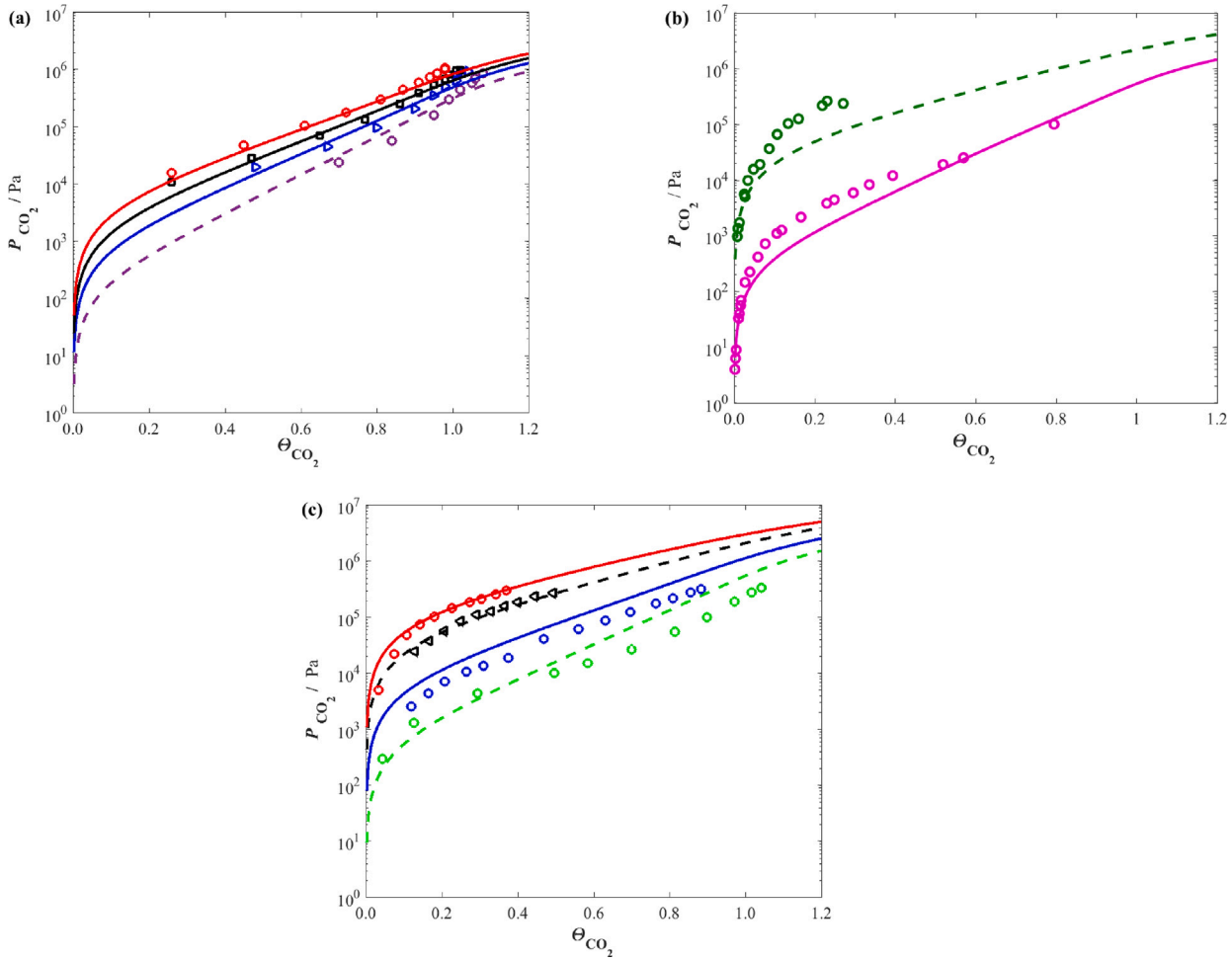

Fig. 15. Isotherms of the vapour–liquid equilibrium of tertiary alkanolamines + H_2O + CO_2 in (a) 24w_{MDEA}% *N*-methyldiethanolamine (MDEA) at T=298.15 K (purple circles [68]), T=313.15 K (blue triangles [68]), T=323.15 K (black squares [68]), and T=333.15 K (red circles [68]); (b) 35w_{MDEA}% *N*-methyldiethanolamine (MDEA) at T= 313.15 K [69] and T= 373.15 K [69]; (c) 30w_{DMMEA}% *N*,*N*-dimethylethanolamine (DMMEA) at T=313.15 K (green circles [70]), T=343.15 K (blue circles [70]), T=373.15 K (black triangles [70]), and T= 393.15 K (red circles) [70]. The symbols represent the experimental data, and the continuous and dotted curves of corresponding colours to calculations and predictions with the SAFT-γ Mie group-contribution approach, respectively.

are considered to be different. Six parameters therefore need to be estimated for each amine group k: ε_{k,CO_2}, λ_{k,CO_2}, $\varepsilon^{HB}_{k,CO_2,e,\alpha_1}$, $\varepsilon^{HB}_{k,CO_2,e,\alpha_2}$, K_{k,CO_2,e,α_2}, and K_{k,CO_2,e,α_2} (k=cNH,CN). The optimized parameters are presented in Tables 4 and 5.

A comparison of the resulting SAFT-γ Mie description of the VLE of the piperazine + water + carbon dioxide mixture with the corresponding experimental data [8] can be seen in Fig. 4 for a range of temperatures (from 313 to 393 K) and amine concentrations (from 1 to 4 molal). The phase diagrams are presented in terms of the partial pressure of CO_2 as a function of CO_2 loading, Θ_{CO_2} (number of moles of CO_2 in the liquid phase/ number of moles of amine in the liquid phase). The adequacy of the approach in describing the CO_2 solubility at both low and high temperatures can be appreciated in the figure. Moreover, we note that only experimental data for the lower concentrations of piperazine (1 and 2 molal) are used in developing the parameters; the data corresponding to the solution of 4 molal PZ is used to test the reliability of the model. As can be seen, a very good description of the experimental data is delivered over the range of temperatures and amine concentrations considered.

In order to develop a suitable model for substituted cyclic amines in which one of the cNH groups of piperazine has been replaced by a cN-R (R ≠ H) moeity, it is necessary to develop unlike interaction parameters for the cN group. The cN-CO_2 group interaction parameters are estimated using isothermal vapour–liquid equilibrium data of aqueous solutions of 30 w% *N*-methylpiperazine (MPZ) with CO_2 at 313.15 K [9]. As in the case of PZ, the interactions between the e site of the nitrogen atom in the cN group and the α_1 and α_2 reactive sites of CO_2 are assumed to interact with different energies, $\varepsilon^{HB}_{cN,CO_2,e,\alpha_s}$ and bonding volume K_{cN,CO_2,e,α_s} (s = 1, 2). The optimized values of the parameters are presented in Tables 4 and 5.

A comparison of the calculated and experimental phase behaviour of aqueous solutions containing *N*-methylpiperazine and *N*-ethylpiperazine (EPZ) and CO_2 is presented in Fig. 5. In addition to the data used in the parameter estimation, aqueous solutions with lower (10w%) and higher (40w%) concentrations of MPZ, and solutions of EPZ are also examined in order to test the predictive transferability of the model parameters. As can be seen in the figure both the calculations and predictions obtained using SAFT-γ Mie are in good agreement with the experimental data in most cases. We note however the larger discrepancy in the prediction of the solubility of CO_2 in the case of the 30w% EPZ solution at 393 K. A temperature-dependent model to treat the association interaction between the e site of the nitrogen atom and the reactive sites of CO_2 would lead to an improvement of the agreement with the high-temperature data; this type of temperature-dependent model has been considered in other versions of the SAFT approach [102–104] but such an approach is not considered here as insufficient data are available to implement this for all groups.

Table 2
SAFT-γ Mie group-interaction matrix for the functional groups considered in our current study. The red shading indicates group interaction parameters developed in the current work; the blue shading indicates group parameters developed in previous work [87,88,99–101]; and the grey shading indicates group interactions derived from the combining rules given in Eqs. (A.1)–(A.7). The lined cells indicate second-order group interaction parameters developed in the current work (red) and those developed previously (blue) [100].

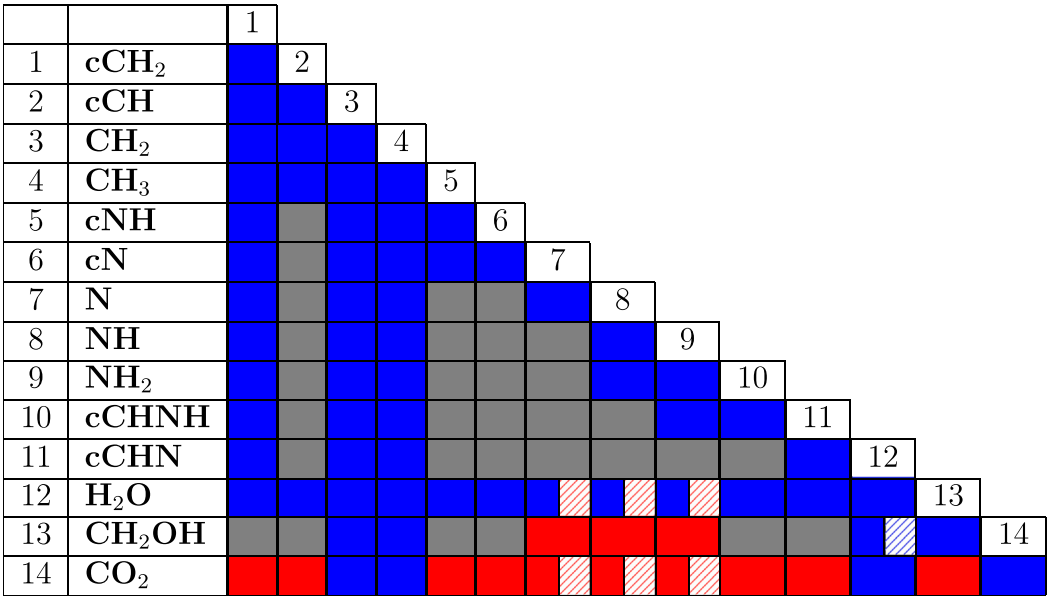

Table 3
Like group parameters for use within the SAFT-γ Mie group-contribution approach: v_k^*, S_k, and σ_{kk} are the number of segments constituting group k, the shape factor, and the segment diameter of group k, respectively; λ_{kk}^r and λ_{kk}^a are the repulsive and attractive exponents, and ε_{kk} is the dispersion energy of the Mie potential characterizing the interaction of two k groups; $N_{ST,k}$ represents the number of association site types on group k, with $n_{k,\mathrm{H}}$, $n_{k,\mathrm{e}}$, n_{k,α_1}, and n_{k,α_2} denoting the number of association sites of type H, e, α_1, and α_2, respectively.

k	Group k	v_k^*	S_k	λ_{kk}^r	λ_{kk}^a	σ_{kk}/Å	$\left(\frac{\varepsilon_{kk}}{k_B}\right)$/K	$N_{ST,k}$	$n_{k,\mathrm{H}}$	$n_{k,\mathrm{e}}$	n_{k,α_1}	n_{k,α_2}	Ref.
1	cCH_2	1	0.24751	20.386	6.0000	4.7852	477.36	–	–	–	–	–	[88]
2	cCH	1	0.096095	8.0000	6.0000	5.4116	699.92	–	–	–	–	–	[87]
3	CH_2	1	0.22932	19.871	6.0000	4.8801	473.39	–	–	–	–	–	[88]
4	CH_3	1	0.57255	15.050	6.0000	4.0773	256.77	–	–	–	–	–	[88]
5	cNH	1	0.16529	19.491	6.0000	4.9810	631.92	2	1	1	–	–	[87]
6	cN	1	0.071900	7.0024	6.0000	4.6120	174.04	1	0	1	–	–	[87]
7	N	1	0.15069	8.8970	6.0000	3.0755	62.971	1	0	1	–	–	[87]
8	NH	1	0.36589	19.999	6.0000	3.2568	100.00	2	1	1	–	–	[87]
9	NH_2	1	0.79675	10.254	6.0000	3.2477	284.78	2	2	1	–	–	[87]
10	cCHNH	1	0.15346	9.2374	6.0000	5.5000	691.56	2	1	1	–	–	[87]
11	cCHN	1	0.10264	8.0016	6.0000	4.4454	709.98	1	0	1	–	–	[87]
12	H_2O	1	1.0000	17.020	6.0000	3.0063	266.68	2	2	2	–	–	[88]
13	CH_2OH	2	0.58538	22.699	6.0000	3.4054	407.22	2	1	2	–	–	[101]
14	CO_2	2	0.84680	26.408	5.0550	3.0500	207.89	2	–	–	1	1	[99]

4.2.3. Linear alkylamine + H_2O + CO_2 mixtures: N–CO_2 , NH–CO_2 and NH_2–CO_2 unlike interaction parameters

Mono-functional linear alkylamines are not used in CO_2 capture, mainly because these substances exhibit a lower reactivity, a lower solubility in water, and a higher vapour pressure than other amines. As a consequence, the experimental data for ternary mixtures of alkylamines with water and carbon dioxide are very limited. Aqueous solutions of alkyl polyamines, which comprise two or more alkylamine groups in their structure, have however been shown to be promising for CO_2 absorption, as the increased number of amine groups leads to higher loadings, with lower vapour pressures, and lower heat of absorption. Moreover, blends of alkylamines and alkanolamines result in phase-change solutions, which are also of current interest. The dialkylamine 3-(methylamino)propylamine (MAPA) [11,13,29,30] and the trialkylamine diethylenetriamine (DETA) [12,105] have been studied in most detail. We use the data available for these systems in the parameter estimation of the unlike interactions between the primary (NH_2), secondary (NH), and tertiary (N) amine groups with CO_2.

As before, the unlike interactions between the α_1 and α_2 reactive sites of CO_2 and the e site of the nitrogen atom present in an amine group l (l = N, NH, NH_2) are assumed to be asymmetric, such that the parameters required to characterize the interactions are: the unlike dispersion energy $\varepsilon_{\mathrm{CO}_2,l}$, the unlike repulsive exponent $\lambda_{\mathrm{CO}_2,l}$, the energies $\varepsilon^{\mathrm{HB}}_{\mathrm{CO}_2,l,\alpha_1,\mathrm{e}}$, $\varepsilon^{\mathrm{HB}}_{\mathrm{CO}_2,l,\alpha_2,\mathrm{e}}$, and bonding volumes $K_{\mathrm{CO}_2,l,\alpha_1,\mathrm{e}}$, $K_{\mathrm{CO}_2,l,\alpha_2,\mathrm{e}}$ of association between reactive sites of type α and sites of type e. The N–CO_2 and NH_2–CO_2 interaction parameters have been presented in previous work [100]. The new unlike interaction parameters between the secondary amine group, NH, and CO_2 are determined using experimental vapour–liquid equilibrium data for aqueous solutions of MAPA (1M concentration) with CO_2 at T =313.15, 353.15, and 393.15 K. The interaction parameters are reported in Tables 4 and 5.

A comparison of the SAFT-γ Mie description and experimental phase behaviour of ternary mixtures of MAPA + H_2O + CO_2 and DETA + H_2O + CO_2 is shown in Fig. 6. Even though the parameters are estimated using experimental data for aqueous solutions of MAPA with concentration 1M only, an accurate prediction of the partial pressures at higher concentrations of MAPA is also observed. Furthermore, as can be seen in Fig. 6(b), the predictions of the solubility of CO_2 in aqueous solutions of DETA are also in good agreement with the experimental values. These results confirm the robustness of the model parameters.

Table 4
Unlike group dispersion energies ϵ_{kl} and repulsive exponent λ^r_{kl} between groups k and l for use within the SAFT-γ Mie group-contribution approach. CR indicates that λ^r_{kl} is obtained from the combining rule given in Eq. (A.3). The dagger symbol (†) indicates that the parameter is developed in the current work.

k	l	Group k	Group l	$\left(\frac{\epsilon_{kl}}{k_B}\right)$/K	λ^r_{kl}	Ref.	k	l	Group k	Group l	$\left(\frac{\epsilon_{kl}}{k_B}\right)$/K	λ^r_{kl}	Ref.
1	2	cCH_2	cCH	321.71	CR	[87]	4	8	CH_3	NH	530.87	CR	[87]
1	3	cCH_2	CH_2	459.67	CR	[88]	4	9	CH_3	NH_2	244.15	CR	[87]
1	4	cCH_2	CH_3	355.95	CR	[88]	4	10	CH_3	cCHNH	406.97	CR	[87]
1	5	cCH_2	cNH	605.45	CR	[87]	4	11	CH_3	cCHN	761.79	CR	[87]
1	6	cCH_2	cN	536.66	CR	[87]	4	12	CH_3	H_2O	358.18	100.00	[101]
1	7	cCH_2	N	650.24	CR	[87]	4	13	CH_3	CH_2OH	333.20	CR	[101]
1	8	cCH_2	NH	549.43	CR	[87]	4	14	CH_3	CO_2	205.70	CR	[99]
1	9	cCH_2	NH_2	332.15	CR	[87]	5	6	cNH	cN	812.26	CR	[87]
1	10	cCH_2	cCHNH	486.88	CR	[87]	5	12	cNH	H_2O	523.83	8.4243	[87]
1	11	cCH_2	cCHN	750.06	CR	[87]	5	14	cNH	CO_2	80.101	39.706	†
1	12	cCH_2	H_2O	350.99	28.000	[87]	6	12	cN	H_2O	2990.0	66.109	[87]
1	14	cCH_2	CO_2	269.68	CR	†	6	14	cN	CO_2	90.102	35.343	†
2	3	cCH	CH_2	522.57	CR	[87]	7	12	N	H_2O	1481.3	21.217	[87]
2	4	cCH	CH_3	690.17	CR	[87]	7	13	N	CH_2OH	440.99	CR	†
2	12	cCH	H_2O	377.16	22.265	[87]	7	14	N	CO_2	100.58	50.000	†
2	14	cCH	CO_2	294.99	CR	†	8	9	NH	NH_2	381.98	CR	[87]
3	4	CH_2	CH_3	350.77	CR	[99]	8	12	NH	H_2O	646.10	13.195	[87]
3	5	CH_2	cNH	429.49	CR	[87]	8	13	NH	CH_2OH	313.25	CR	†
3	6	CH_2	cN	508.54	CR	[87]	8	14	NH	CO_2	100.01	49.529	†
3	7	CH_2	N	348.30	CR	[87]	9	10	NH_2	cCHNH	101.61	CR	[87]
3	8	CH_2	NH	394.58	CR	[87]	9	12	NH_2	H_2O	358.55	CR	[87]
3	9	CH_2	NH_2	348.39	CR	[87]	9	13	NH_2	CH_2OH	528.21	52.305	†
3	10	CH_2	cCHNH	309.95	CR	[87]	9	14	NH_2	CO_2	200.62	49.975	†
3	11	CH_2	cCHN	893.50	CR	[87]	10	12	cCHNH	H_2O	855.01	32.132	[87]
3	12	CH_2	H_2O	423.63	100.00	[101]	10	14	cCHNH	CO_2	100.52	31.233	†
3	13	CH_2	CH_2OH	423.17	CR	[101]	11	12	cCHN	H_2O	1067.9	8.0010	[87]
3	14	CH_2	CO_2	276.45	CR	[99]	11	14	cCHN	CO_2	161.38	33.269	†
4	5	CH_3	cNH	583.72	CR	[87]	12	13	H_2O	CH_2OH	353.37	CR	[101]
4	6	CH_3	cN	710.00	CR	[87]	12	14	H_2O	CO_2	226.38	CR	[99]
4	7	CH_3	N	462.18	CR	[87]	13	14	CH_2OH	CO_2	312.30	CR	†

The heat of absorption, which is obtained by summing the heats of dissolution and of reaction, is an important property to consider in the design of new solvent systems as it has a direct impact on the amount of energy needed to regenerate the solvent. In order to validate further the reliability of the interaction parameters between the alkylamine groups and CO_2, we predict the differential heat of absorption in aqueous solutions of MAPA, in terms of the enthalpy change ($-\Delta H_{abs}$), as function of the CO_2 loading in the liquid phase at VLE conditions as described in [106]. As can be seen in Fig. 7, a good agreement with experimental data is observed. Although no experimental data are available in the case of DETA, SAFT-γ Mie predictions are also presented in the figure for this system.

4.3. CO_2 solubility in aqueous solutions of alkanolamines

Alkanolamines contain both alcohol and amine groups. These compounds are often used in the context of CO_2 capture, as the presence of the hydroxyl group serves to reduce the solvent vapour pressure and increase the solubility in water. In order to develop a model suitable for the study of the phase behaviour of aqueous solutions of alkanolamines with CO_2, it is essential to account for the multi-functional nature of alkanolamines, including the effects of the interactions of the hydroxyl and amine groups with water, and of the close proximity of these two groups within alkanolamine molecules. In the context of the SAFT-γ Mie group-contribution approach these effects can be taken into account by employing second-order group interactions [79,100]. Specifically, we introduce second-order interactions to model the unlike interactions between the NH_2, NH, and N groups and H_2O when the amine group is in close proximity to a hydroxyl group within the alkanolamine structure.

4.3.1. Primary, secondary and tertiary pure alkanol amines: NH_2–CH_2OH, NH–CH_2OH, and N–CH_2OH unlike interaction parameters

Alkanolamine molecules of interest in our work comprise NH_2, NH, or N amine groups, the methyl hydroxyl group CH_2OH, and a number of CH_2 and CH_3 groups. The interactions between the amine groups and the alkyl group, as well as the CH_2OH–CH_2 and CH_2OH–CH_3 interactions have been presented in previous work [101]. The first-order NH_2–CH_2OH, NH–CH_2OH, and N–CH_2OH interactions are estimated here using experimental data for pure alkanolamines. We also note that the N–CH_2OH determined in our current work has been successfully tested in the modelling of mixtures including choline [107,108].

For the interactions involving NH_2 and CH_2OH, we use vapour-pressure and saturated-liquid-density data for monoethanolamine (MEA) and 3-amino-1-propanol (MPA), as well as isobaric heat-capacity data for the liquid phase of pure MEA and MPA. Similarly, the unlike interactions between the groups NH and CH_2OH are obtained using vapour-pressure, saturated-liquid-density, and isobaric heat-capacity data for diethanolamine (DEA). The CH_2OH group includes one site of type H and two sites of type e, while the amine groups include one site of type e due to the presence of the nitrogen atom, and one or two sites of type H, depending on the number of hydrogens present. Consequently, in the case of NH_2 and NH groups, a set of six parameters has to be determined: ϵ_{k,CH_2OH}, λ^r_{k,CH_2OH}, $\epsilon^{HB}_{k,CH_2OH,H,e}$, $K_{k,CH_2OH,H,e}$, $\epsilon^{HB}_{k,CH_2OH,e,H}$, $K_{k,CH_2OH,e,H}$; k = NH_2, NH.

In the case of the tertiary alkyl amine group N only four parameters need to be specified, as this group does not have an H site [87]. The unlike interactions between groups N and CH_2OH (ϵ_{N,CH_2OH}, λ^r_{N,CH_2OH}, $\epsilon^{HB}_{N,CH_2OH,e,H}$, $K_{N,CH_2OH,e,H}$) are determined using experimental data for pure N-methyldiethanolamine (MDEA) including the vapour pressure, the saturated-liquid density, and the liquid-phase heat capacity.

The optimal values obtained for the unlike NH_2–CH_2OH, NH–CH_2OH, and N–CH_2OH group interactions are given in Tables 4 and 5. The calculated fluid-phase coexistence properties and the isobaric heat capacity (C^L_p) for liquid MEA, MPA, DEA, and MDEA are compared with available experimental data [109–117] in Table 8. As can be gleaned from the absolute average deviations %AAD, very good agreement between theory and experiment is obtained for the primary alkanolamines MEA and MPA. For DEA, a good description of the vapour pressure and saturated-liquid density are achieved, with slightly larger deviations in the liquid heat capacity, C^L_p. Deviations in the description of the

Table 5
Group association energy $\varepsilon^{HB}_{kl,ab}$ and bonding volume $K_{kl,ab}$ parameters describing the interaction between site type a on group k and site type b on group l for use within the SAFT-γ Mie group-contribution approach. The dagger symbol (†) indicates that the parameter is developed in the current work.

k	l	Group k	Site a of group k	Group l	Site b of group l	$\left(\frac{\varepsilon^{HB}_{kl,ab}}{k_B}\right)$/K	$K_{kl,ab}$/Å^3	Ref.
5	5	cNH	e	cNH	H	1511.6	87.651	[87]
5	6	cNH	H	cN	e	901.35	1.1555	[87]
5	12	cNH	H	H_2O	e	1701.0	1.6177	[87]
5	12	cNH	e	H_2O	H	2838.4	37.395	[87]
5	14	cNH	e	CO_2	α_1	5696.6	4.6758	†
5	14	cNH	e	CO_2	α_2	6017.9	1.1003	†
6	12	cN	e	H_2O	H	5203.7	0.037400	[87]
6	14	cN	e	CO_2	α_1	3388.6	1031.0	†
6	14	cN	e	CO_2	α_2	3004.9	659.21	†
7	12	N	e	H_2O	H	2783.7	15.536	[87]
7	13	N	e	CH_2OH	H	1247.2	286.83	†
7	14	N	e	CO_2	α_1	4270.8	0.46340	†
7	14	N	e	CO_2	α_2	7439.8	0.0067500	†
8	8	NH	e	NH	H	1370.3	10.062	[87]
8	9	NH	H	NH_2	e	1682.1	0.58200	[87]
8	9	NH	e	NH_2	H	1639.9	37.900	[87]
8	12	NH	H	H_2O	e	1064.5	400.82	[87]
8	12	NH	e	H_2O	H	3890.4	928.00	[87]
8	13	NH	H	CH_2OH	e	341.13	1499.8	†
8	13	NH	e	CH_2OH	H	1390.1	947.93	†
8	14	NH	e	CO_2	α_1	6012.1	0.14157	†
8	14	NH	e	CO_2	α_2	7420.5	0.43534	†
9	9	NH_2	e	NH_2	H	1,070.8	95.225	[87]
9	12	NH_2	e	H_2O	H	1460.0	179.60	[87]
9	12	NH_2	H	H_2O	e	1,988.3	55.824	[87]
9	13	NH_2	H	CH_2OH	e	629.88	346.08	†
9	13	NH_2	e	CH_2OH	H	2403.8	26.192	†
9	14	NH_2	e	CO_2	α_1	4023.9	120.35	†
9	14	NH_2	e	CO_2	α_2	5981.4	1.0036	†
10	10	cCHNH	e	cCHNH	H	1293.5	438.49	[87]
10	12	cCHNH	H	H_2O	e	5477.7	0.0095820	[87]
10	12	cCHNH	e	H_2O	H	5903.8	0.0020750	[87]
10	14	cCHNH	e	CO_2	α_1	2246.0	0.14056	†
10	14	cCHNH	e	CO_2	α_2	3870.8	6445.7	†
11	12	cCHN	e	H_2O	H	4115.4	0.23070	[87]
11	14	cCHN	e	CO_2	α_1	4114.9	4686.4	†
11	14	cCHN	e	CO_2	α_2	1013.9	1551.7	†
12	12	H_2O	H	H_2O	e	1985.4	101.69	[88]
12	13	H_2O	e	CH_2OH	H	621.68	425.00	[101]
12	13	H_2O	H	CH_2OH	e	2153.2	147.40	[101]
12	14	H_2O	e	CO_2	α_1	1398.1	91.419	[99]
13	13	CH_2OH	H	CH_2OH	e	2097.9	62.309	[101]

Table 6
Second-order unlike group dispersion interaction energies ε_{kl} and repulsive exponent λ^r_{kl} between groups k and l. When group k is present in the molecular environment indicated by the square brackets, the parameters in the table are used instead of those presented in Tables 4 and 5; see Section 4.3 for details. The dagger symbol (†) indicates that the parameter is developed in the current work. R=CH_3, NH_2, NH, N; R_1 = CH_3, CH_2CH_2OH.

k	l	Group k	Group l	Molecular environment of group k	$\left(\frac{\varepsilon_{kl}}{k_B}\right)$/K	λ^r_{kl}	Ref.
13	12	CH_2OH	H_2O	[R$(CH_2)_n$]CH_2OH; n=0,1,2 (excluding butanol)	358.02	CR	[100]
9	12	NH_2	H_2O	$NH_2[(CH_2)_n$ $(CH_2OH)]$; n=1,2	339.89	CR	†
9	14	NH_2	CO_2	$NH_2[(CH_2)_n$ $(CH_2OH)]$; n=1,2	134.58	50.060	†
8	12	NH	H_2O	$[NHCH_2CH_2OH]_2$	488.28	49.901	†
8	14	NH	CO_2	$[NHCH_2CH_2OH]_2$	90.008	49.983	†
7	12	N	H_2O	$R_1CH_3N[CH_2CH_2OH]$	1569.8	37.928	†
7	14	N	CO_2	$R_1CH_3N[CH_2CH_2OH]$	241.18	CR	†

vapour pressure are slightly higher for ternary amine MDEA, but C^L_p is reproduced very accurately. Deviations for dimethylmonoethanolamine (DMMEA) are also included in the table. No experimental data for this compound are included in the characterization of groups, so that the good level of agreement reported in the table provides evidence of the reliability of the group interactions. Phase diagrams comparing the available pure-compound experimental data and our SAFT-γ Mie calculations for each of the alkanolamines discussed are also presented in Appendix D.

4.3.2. Alkanolamine + H_2O mixtures: NH_2–H_2O, NH–H_2O, and N–H_2O second-order interactions in an environment of hydroxyl groups

In order to model the thermodynamic properties of aqueous solutions of alkanolamines, amine–water and hydroxyl–water group interactions need to be characterized. All of the relevant groups can be found in Tables 6 and 7. The parameters accounting for the interactions between the CH_2OH and H_2O groups have been presented previously [100]. Here, we are interested in modelling short-chain alkanolamines, and second-order interactions between these groups are used to improved the accuracy of the description. In order to account for the polarization of the amine groups in the presence of the hydroxyl group and of water, we find that second-order interactions for each of the amine–water group interactions (NH_2–H_2O, NH–H_2O, N–H_2O) are needed for a good description of the phase behaviour of aqueous solutions of short alkanolamines. Finally, the CH_2–H_2O interactions have been presented in previous work [101] and are transferred directly without the need for second-order refinement.

Table 7
Second-order unlike group association energies $\epsilon^{HB}_{kl,ab}$ and bonding-volumes $K_{kl,ab}$ between site type a on group k and site type b on group l. When group k appears in the molecular environment indicated by the square brackets, the parameters in this table are used instead of those presented in Tables 4 and 5; see Section 4.3 for details. The dagger symbol (†) indicates that the parameter is developed in the current work. R= CH_3, NH_2, NH, N; R_1 = CH_3, CH_2CH_2OH.

k	l	Group k	Site a of group k	Group l	Site b of group l	Molecular environment of group k	$\left(\frac{\epsilon^{HB_{kl}}}{k_B}\right)$/K	$K_{kl,ab}$/Å^3	Ref.
13	12	CH_2OH	H	H_2O	e	$[R(CH_2)_n]CH_2OH$; n=0,1,2 (excluding butanol)	600.00	490.19	[100]
13	12	CH_2OH	e	H_2O	H	$[R(CH_2)_n]CH_2OH$; n=0,1,2 (excluding butanol)	2000.6	130.02	[100]
9	12	NH_2	e	H_2O	H	$NH_2[(CH_2)_n\ (CH_2OH)]$; n=1,2	1877.5	459.18	†
9	12	NH_2	H	H_2O	e	$NH_2[(CH_2)_n\ (CH_2OH)]$; n=1,2	1364.4	22.450	†
9	14	NH_2	e	CO_2	α_1	$NH_2[(CH_2)_n\ (CH_2OH)]$; n=1,2	3313.0	3280.3	†
9	14	NH_2	e	CO_2	α_2	$NH_2[(CH_2)_n\ (CH_2OH)]$; n=1,2	4943.6	142.64	†
8	12	NH	e	H_2O	H	$[NHCH_2CH_2OH]_2$	305.80	0.011099	†
8	12	NH	H	H_2O	e	$[NHCH_2CH_2OH]_2$	1756.2	24.260	†
8	14	NH	e	CO_2	α_1	$[NHCH_2CH_2OH]_2$	7020.9	0.017360	†
8	14	NH	e	CO_2	α_2	$[NHCH_2CH_2OH]_2$	2490.6	686.82	†
7	12	N	e	H_2O	H	$R_1CH_3N[CH_2CH_2OH]$	2876.5	0.84013	†
7	14	N	e	CO_2	α_1	$R_1CH_3N[CH_2CH_2OH]$	5500.7	1.3695	†
7	14	N	e	CO_2	α_2	$R_1CH_3N[CH_2CH_2OH]$	3437.4	2.7670	†

Table 8
Absolute average deviations %AAD from experimental values for the vapour pressure, P_{vap}, the saturated-liquid density, ρ_{sat}, and the liquid-phase isobaric specific heat capacity, C_p^L, of MEA, MPA, DEA, MDEA, and DMMEA. The number of data points N_p used for each property p and the temperature range considered are also reported.

Compound	T/K	N_P	% AAD[P_{vap}]	Ref.	T/K	N_ρ	% AAD[ρ_{sat}]	Ref.	T/K	$N_{C_p^L}$	% AAD[C_p^L]	Ref.
MEA	325–443	23	1.44	[109]	301–432	34	0.16	[110]	303–393	10	1.76	[111]
MPA	372–531	27	2.12	[112]	311–593	19	0.13	[112]	303–393	21	2.35	[111,113]
DEA	380–720	18	2.06	[114]	380–720	20	1.99	[114]	301–353	19	8.16	[114]
MDEA	409–543	21	29.12	[115]	316–661	14	3.99	[117]	303–393	10	0.50	[116]
DMMEA	274–365	12	12.25	[56]	260–570	16	4.50	[56]	–	–	–	–

The second-order interactions between the NH_2 and H_2O groups in molecular environments containing the short-chain alcohol group CH_2OH are determined using experimental data for isothermal and isobaric VLE of aqueous solutions of MEA [14,15] and of MPA [16], and the resulting description is shown in Fig. 8. The optimal values estimated for the second-order NH_2–H_2O interaction are given in Tables 6 and 7. The square brackets in $NH_2[(CH_2)_nCH_2OH]$ indicate that the parameters relate to the NH_2 group when bonded to the moiety in the brackets, i.e., in a specific molecular environment, where n corresponds to the number of methylene (CH_2) groups of the molecule; i.e., $n = 1$ for MEA, and $n = 2$ for MPA.

The second-order interactions between the NH and H_2O groups are developed using experimental information for aqueous solutions of diethanolamine (DEA), i.e., isothermal [18] and isobaric vapour–liquid equilibria [19,20] data. The optimal values for the second-order unlike-interaction parameters are summarized in Tables 6 and 7. The resulting description of the fluid-phase behaviour of binary mixtures of DEA + water is presented in Fig. 9. The corresponding use of these second-order interactions is represented as $NH[CH_2CH_2OH]_2$–H_2O in the tables. In this case the molecular environment indicated with the square brackets between the NH and H_2O is characterized by the presence of two short-chain ethylalcohols.

Finally, the second-order group interactions between the water group and the tertiary amine group N are derived to model the equilibrium properties of aqueous solutions of tertiary alkanolamines. The molecular environment is described by $[R_1CH_3]N[CH_2CH_2OH]$, where R_1 can represent either a methyl substituent (the CH_3 group) as for N,N-dimethylmonoethanolamine, or another short-chain ethylalcohol $[CH_2CH_2OH]$, as for methyldiethanolamine. Vapour–liquid equilibrium data of aqueous solutions of methyldiethanolamine (MDEA) [53–55] and N,N-dimethylmonoethanolamine (DMMEA) [56] are used in the parameter estimation. The optimized parameters are reported in Tables 6 and 7, together with examples of the use of second-order groups. The adequacy of the approach is clearly apparent from Fig. 10. We also assess the robustness of the group interactions by predicting the excess enthalpies of mixing (which are not included in the parameterization procedure) of methyldiethanolamine (MDEA) + H_2O and N,N-dimethylmonoethanol amine (DMMEA) + H_2O mixtures. A comparison of the experimental data available [57,58] with our SAFT-γ Mie predictions is presented in Fig. 11. As can be seen, a very good level of agreement is obtained.

The second-order group parameters presented here characterize the interactions in aqueous solutions of short-chain alkanolamines, in which there is a notable polarization effect due to the proximity of the hydroxyl and amine groups. These interactions have only been tested in the environments described in Tables 6 and 7. We do not expect these interactions to be transferable to larger molecules where the proximity of the hydroxyl group is expected to have a less significant effect.

4.3.3. Alkanolamine + H_2O + CO_2 mixtures: CH_2OH–CO_2, NH_2–CO_2, NH–CO_2, and N–CO_2 second-order interactions

Having determined the unlike interaction parameters allowing us to describe the effect of the proximity of hydroxyl groups on the interactions between alkylamine groups and H_2O, we consider the interactions of the amine groups with CO_2 in the same molecular environments. We start our analysis by determining the unlike interactions between the CO_2 and CH_2OH group, using experimental data of binary mixtures of linear alcohols and carbon dioxide. Note that first-order interactions are used for both groups, as there is no water present. We assume that no association occurs between CO_2 and the CH_2OH group. Only the unlike dispersion energy $\epsilon_{CH_2OH\text{-}CO_2}$ is adjusted, using experimental isothermal VLE data of binary mixtures of carbon dioxide with ethanol [59] and 1-propanol [60]. The unlike repulsive-range parameter $\lambda^r_{CH_2OH\text{-}CO_2}$ is determined using the combining rule given in Eq. (A.3). The optimized unlike interaction parameters are presented in Table 5, and the resulting SAFT-γ Mie description of the VLE for the ethanol + carbon dioxide and propanol + carbon dioxide mixtures are compared to the experimental data in Fig. 12. For both alcohols, the presence of a region of liquid–liquid demixing at higher pressures is predicted with the SAFT-γ Mie model. Although there are no data on LLE for these systems, Lam et al. [118] have observed VLLE for the mixtures of CO_2 mixture linear alcohols from propanol to n-hexanol. Their experiments did not identify any region of liquid–liquid immiscibility for the CO_2 +

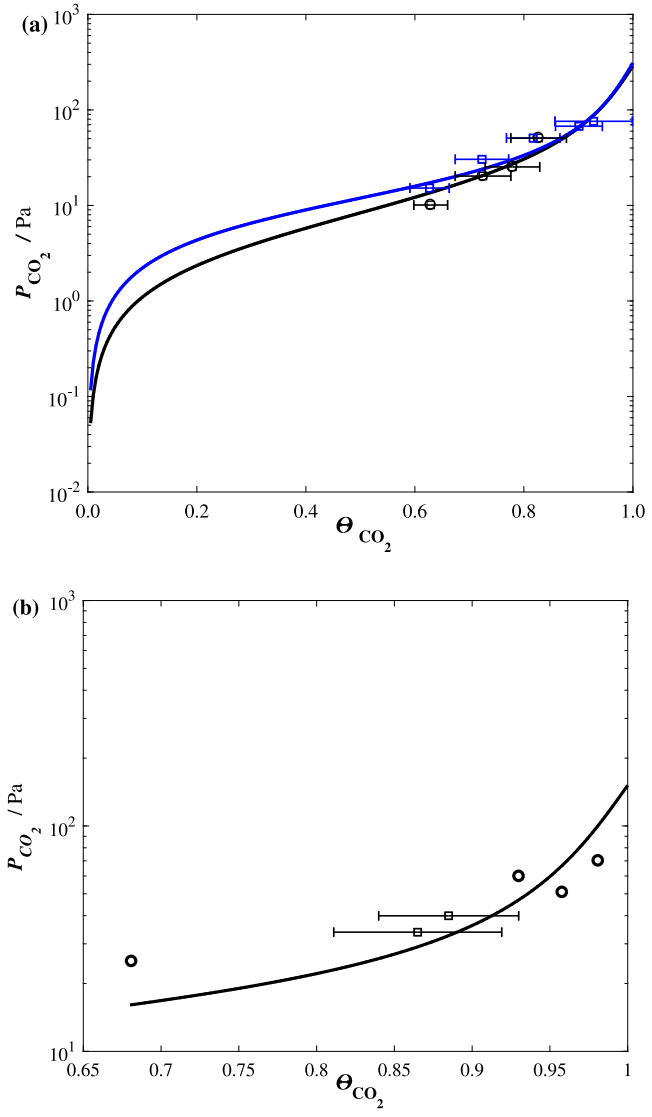

Fig. 16. Isotherms of the fluid-phase behaviour of cyclohexylamines + H_2O + CO_2 as a function of CO_2 loading in (a) $\approx 35.5 w_{MCA}\%$ at T = 313.15 K (black circles) and T = 333.15 K (blue squares), and (b) $\approx 26.7 w_{DMCA}\%$ at T = 313.15 K (black squares) and data of Tan et al. [76] (black circles). All curves correspond to calculations with the SAFT-γ Mie group-contribution approach.

ethanol mixture. The prediction of immiscibilty in the latter mixture are likely a result of the overprediction of the LLE region with our models.

In order to model the thermodynamic properties of aqueous solutions of alkanolamines and CO_2, second-order interactions between the amine groups in alkanolamines and CO_2 are developed using relevant experimental data, treating the association between the reactive α_1 and α_2 sites of CO_2 and the association sites of the amine groups as asymmetric. The parameters for the second-order interactions between the NH and CO_2 groups were presented in previous work [100]. The unlike parameters characterizing the second-order interactions between NH_2 and CO_2 in primary alkanolamines are obtained using experimental vapour–liquid equilibrium data of aqueous solutions of $30w\%$ monoethanolamine (MEA) with CO_2, at T = 298.15 K and 313.15 K [65]. The resulting second-order unlike group interaction parameters are presented in Tables 6 and 7. In Fig. 13, the available experimental data for the variation of the partial pressure of CO_2 with the CO_2 loading in aqueous solutions of MEA and DEA are compared with SAFT-γ Mie calculations. Although the estimation of the parameters is based on two isotherms and only one alkanolamine, very good predictions of the phase behaviour at higher temperatures are obtained for both systems.

In order to test the reliability of the implicit approach accounting for the chemical speciation that occurs during the absorption of CO_2 in aqueous solutions of MEA and DEA, we calculate the equilibrium concentrations of the carbamate and bicarbonate species, following a statistical analysis [78,79,119] of the fractions of CO_2 molecules not bonded at sites α_1 and α_2 which are calculated within the association term of the SAFT-γ Mie equation (see Eqs. (5) and (6)).

As detailed in Section 2.2, a carbamate molecule is formed according to reaction (7), so that both α_1 and α_2 sites of CO_2 are bonded, and the corresponding concentration can be obtained using Eq. (10). Similarly, bicarbonate is formed according to reaction (8), when one of α_1 and α_2 sites is bonded. The corresponding concentration of bicarbonate is given by Eq. (11). The concentration of free (molecular) CO_2, in solution $x^*_{CO_2}$ is obtained from the fraction of CO_2 molecules not bonded any site, i.e., [79,119]

$$x^*_{CO_2} = x_{CO_2} X_{CO_2,CO_2,\alpha_1} X_{CO_2,CO_2,\alpha_2} \tag{14}$$

A comparison of the calculated and measured mole fractions of carbamate, bicarbonate, and molecular CO_2 as a function of CO_2 loading in the MEA + H_2O + CO_2 [45,67] and DEA + H_2O + CO_2 mixtures [45] is presented in Fig. 14. Very good agreement between theory and experiment is apparent for both systems at the temperatures considered. It is worth emphasizing that this accurate characterization of the degree of chemical speciation of the mixture has been obtained without speciation data, information for the chemical equilibrium constants, or a detailed reaction mechanism. The ability to predict the molecular speciation is a major benefit of the implicit approach to reaction modelling within the proposed framework. Note that it would also be possible to develop SAFT-γ Mie models that include an explicit treatment of the reactions and speciation, drawing on recent work on the modelling of strong and weak electrolytes [120,121].

We conclude this section by presenting the set of second-order parameters developed to describe the unlike interaction between the tertiary amine group, N, and CO_2 in aqueous solutions of short-chain alkanolamines. We use experimental data for the partial pressure of CO_2 as a function of CO_2 loading in aqueous solutions of two ternary alkanolamines: N-methyldiethanolamine (MDEA), which contains two hydroxyl functional groups, and N,N-dimethylethanolamine (DMMEA), with one hydroxyl functional group. The approach implemented for the unlike interactions of secondary and primary alkanolamines with CO_2 is followed, where the acceptor (reactive) sites of CO_2 are considered to be different and therefore a total of six parameters are needed to characterize these second-order interactions: $\epsilon_{N,CO_2}, \lambda^r_{N,CO_2}, \epsilon^{HB}_{N,CO_2,e,\alpha_s}, K_{N,CO_2,e,\alpha_s}$ (for s=1,2). Experimental CO_2 solubility data at varying conditions of solvent composition, pressure and temperature are used to optimize these parameters. The resulting second-order group interactions parameters are presented in Tables 6 and 7. A comparison of the experimental partial pressures of CO_2 as a function of loading and the description obtained with the SAFT-γ Mie is presented in Fig. 15. As can be seen, very good agreement is generally observed between the experimental data and calculated values, although larger deviations are apparent for the $35w_{MDEA}\%$ MDEA solution.

4.4. CO_2 solubility in aqueous mixtures of cyclohexylamines

In previous work [87] we modelled the fluid-phase behaviour of aqueous solutions of N,N-dimethyl cyclohexylamine (DMCA), N-ethylcyclohexylamine (ECA), and N-methylcyclohexylamine (MCA) which exhibit liquid–liquid equilibria bounded by lower critical solution temperatures (LCSTs). Here, we extend the analysis to treat biphasic aqueous solutions of cyclohexylamines loaded with CO_2 in order to assess their potential as phase-change solvents. We present new

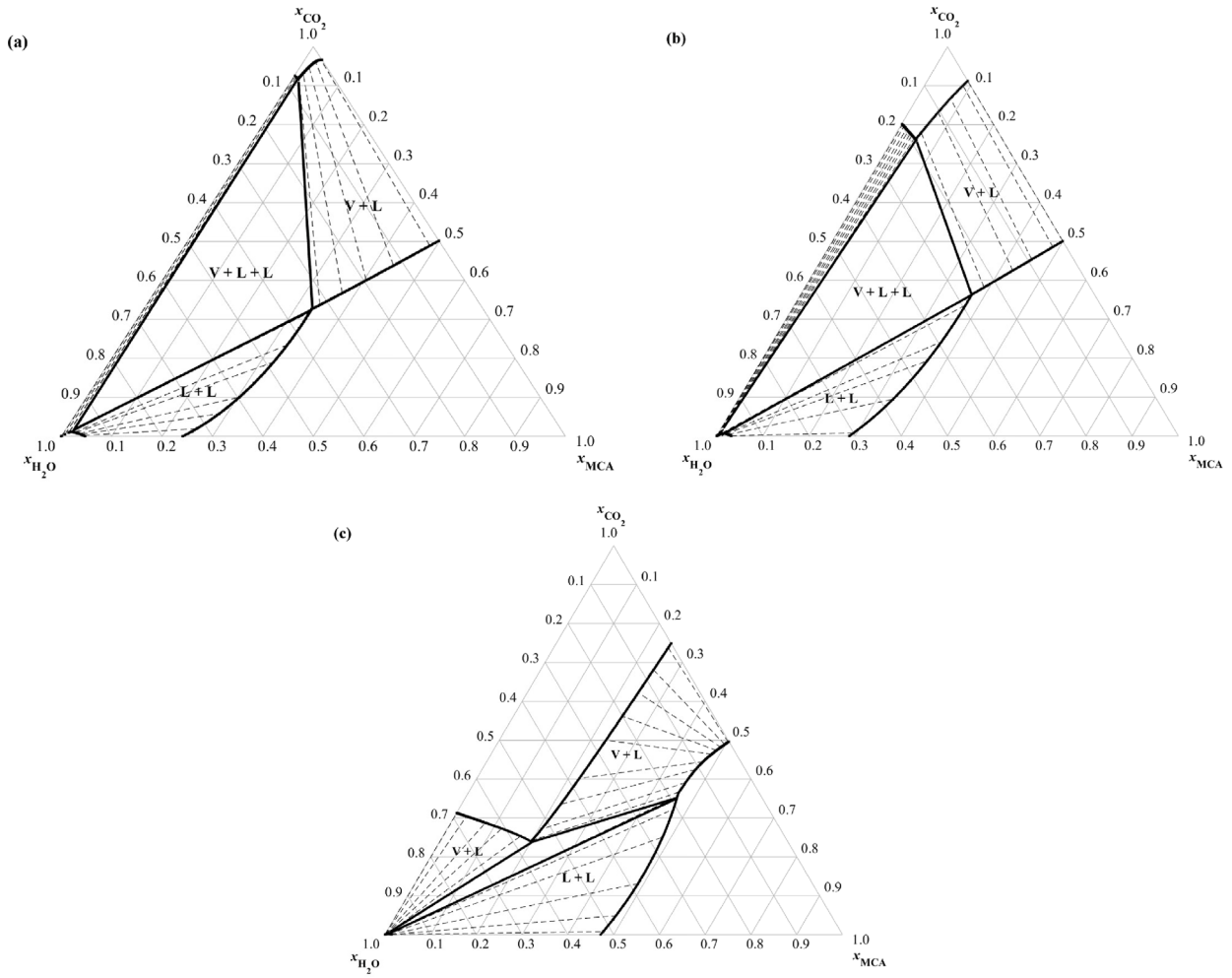

Fig. 17. The ternary phase diagrams of MCA + H_2O + CO_2 mixtures at P = 1.01 bar and (a) T= 313.15 K, (b) T= 333.15 K, and (c) T= 363.15 K, predicted using the SAFT-γ Mie group-contribution approach. The two-phase boundaries, vapour + liquid (V+L) and liquid + liquid (L+L), are depicted using continuous curves and the corresponding tie lines are shown as dashed lines. A three-phase vapour + liquid + liquid (V+L+L) triangular region can also be seen enclosed by solid lines.

experimental measurements of the phase behaviour of these mixtures, obtained following the procedure described in Section 3.2, and use these data to characterize the cCNH–CO_2 and cCN–CO_2 unlike interaction parameters necessary to model the phase behaviour of these mixtures with the SAFT-γ Mie approach.

4.4.1. Experimental results

Experimental measurements of the partial pressure and CO_2 loading in mixtures of MCA + H_2O + CO_2 were carried out at 313.15, 333.15, and 363.15 K, starting from an aqueous amine solution with 40w% amine. The data measured are presented in Table 9. We find that the mixture loaded with CO_2 only exhibits vapour–liquid equilibrium (VLE), with a single, homogeneous, liquid phase for the entire range of pressures considered at 313.15 and 333.15 K. However, at 363.15 K, while VLE is observed at CO_2 partial pressures above 30 kPa, at partial pressures below 25 kPa vapour–liquid–liquid equilibrium (VLLE) is seen. The data corresponding to the partial pressure of CO_2 over a homogeneous liquid phase of loaded aqueous solutions of MCA are presented in Fig. 16(a).

Measurements were also performed for DMCA + H_2O + CO_2 mixtures, at 313.15, 333.15, and 363.15 K, starting from a 3 M aqueous solution of DMCA. The concentrations and partial pressures measured are presented in Table 10. Most of the states considered are found to exhibit VLLE, except for those at the higher partial pressures and 313.15 K. The data corresponding to 313.15 K are presented as a phase diagram in Fig. 16(b), where a comparison with literature data [76] is also provided. As can be seen from the figure, our measured data are in good agreement with the published data.

4.4.2. SAFT-γ Mie calculations: cCHNH–CO_2 and cCHN-CO_2 interactions

The cCHNH–CO_2 and cCHN–CO_2 unlike interactions are determined using the experimental data for the partial pressure of CO_2 over aqueous solutions of N–methylcyclohexylamine (MCA) and N,N–dimethylcyclohexylamine (DMCA) described in the previous section. We use only experimental points corresponding to states exhibiting VLE with a homogeneous (single phase) liquid. More specifically, these correspond to the data measured at T = 313.15 K and T = 333.15 K in the case of MCA solutions (Table 9) and T=313.15 K for DMCA solutions (Table 10). As with other amine groups, the interactions between the association sites of the amine groups and the reactive sites of CO_2 (α_1 and α_2) are treated as asymmetric. Hence, six parameters are required to describe the cCHNH–CO_2 and cCHNH–CO_2 unlike interactions: ε_{k,CO_2}, λ^r_{k,CO_2}, $\varepsilon^{HB}_{k,CO_2,e,\alpha_s}$, K_{k,CO_2,e,α_s} (for k=cCHNH, cCHN, and s=1,2). The corresponding parameters are reported in Tables 4 and 5. A comparison of the experimental and calculated data can be seen in Fig. 16, where our SAFT-γ Mie model found to allow for a very good description of the CO_2 solubility in these mixtures.

It is also of interest to represent the fluid-phase behaviour of these systems in terms of ternary phase diagrams at a specified pressure and temperature over the entire composition range, as understanding the

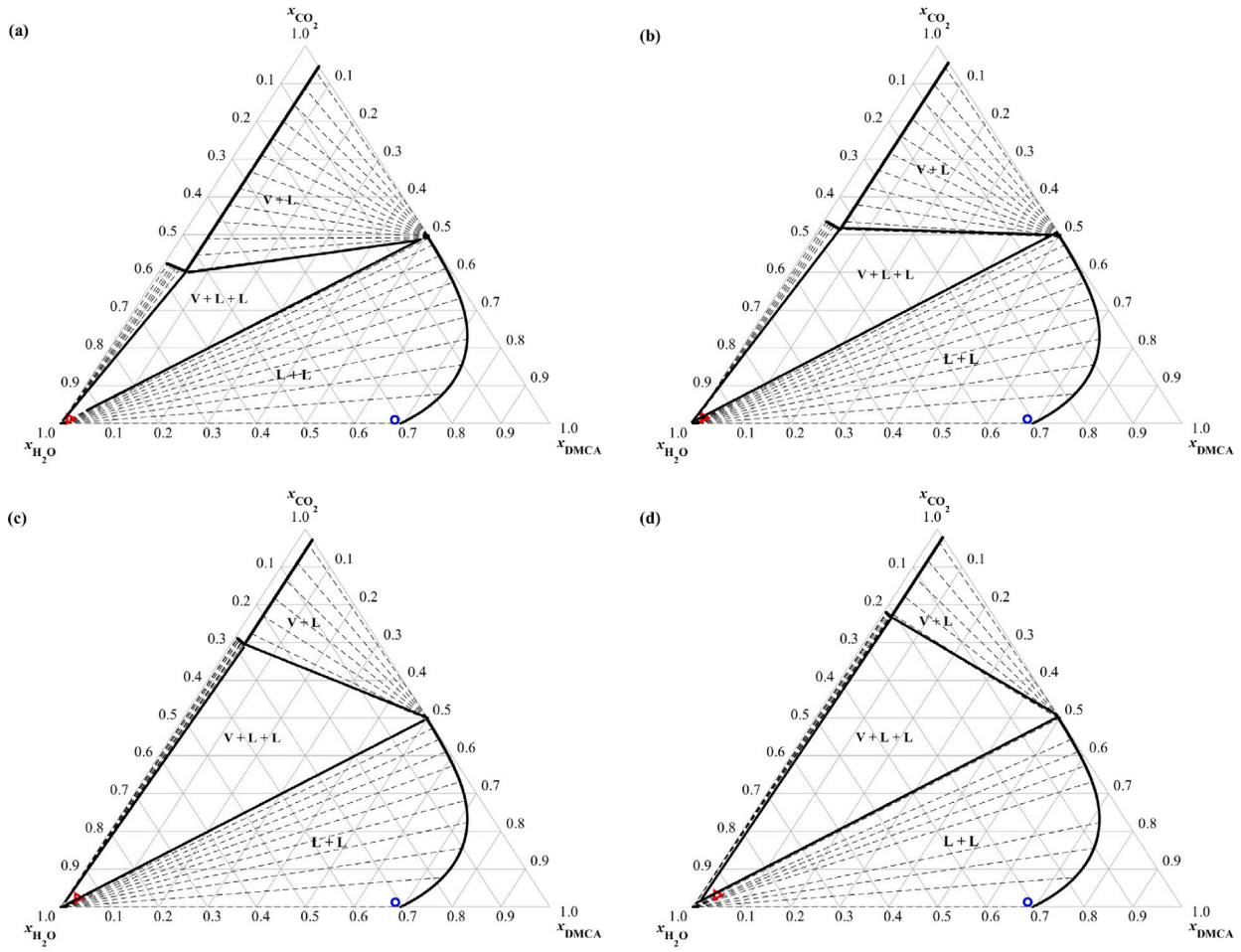

Fig. 18. The ternary phase diagrams for the DMCA + H_2O + CO_2 mixture at T = 333.15 K and total pressure of (a) P = 0.34 bar, (b) P = 0.42 bar, (c) P = 0.69 bar and (d) P = 0.91 bar, predicted using the SAFT-γ Mie group-contribution approach. The symbols correspond to experimental data measured in our current work (cf. Table 10). Two-phase boundaries, vapour + liquid (V+L) and liquid + liquid (L+L), are depicted using continuous curves and the corresponding tie lines are represented by dashed lines. A three-phase vapour + liquid + liquid equilibria (V+L+L) triangular region can be seen enclosed by solid lines.

Table 9
The measured CO_2 solubility in aqueous MCA solutions (40w% of amine). Θ_{CO_2} represents the CO_2 loading, defined as the number of moles of CO_2 in the corresponding liquid phase per mole of amine in that phase. In cases of VLLE, data for the upper (U, organic) and lower (L, aqueous) phases are reported. The * indicates that the final amine content is expressed on a water basis.

T/K	P_{CO_2} /kPa	Phase equilibria	Θ_{CO_2}	Final amine content* w_{amine}%
313.15	10.1	VLE	0.629 ± 0.031	35.9 ± 0.6
313.15	20.3	VLE	0.725 ± 0.051	35.6 ± 0.6
313.15	25.3	VLE	0.779 ± 0.050	34.4 ± 0.6
313.15	50.7	VLE	0.827 ± 0.051	35.0 ± 0.6
333.15	15.2	VLE	0.627 ± 0.036	38.6 ± 0.7
333.15	30.4	VLE	0.723 ± 0.049	33.4 ± 0.6
333.15	50.7	VLE	0.817 ± 0.049	33.7 ± 0.6
333.15	67.5	VLE	0.901 ± 0.043	31.8 ± 0.5
333.15	76.0	VLE	0.928 ± 0.071	33.1 ± 0.5
363.15	18.1	VLLE (U)	0.042 ± 0.003	67.4 ± 1.1
363.15	18.1	VLLE (L)	0.277 ± 0.041	13.3 ± 0.3
363.15	25.1	VLLE (U)	0.073 ± 0.005	59.0 ± 1.0
363.15	25.1	VLLE (L)	0.398 ± 0.039	8.3 ± 0.2
363.15	33.8	VLE	0.262 ± 0.013	34.7 ± 0.6
363.15	50.7	VLE	0.313 ± 0.013	36.8 ± 0.6

relationship between miscibility, solvent composition, and CO_2 loading is instrumental in making an appropriate solvent choice for the design of the capture process. The number and type of phases coexisting at equilibria predicted by our SAFT-γ Mie model are presented in Figs. 17 and 18 for MCA + H_2O + CO_2 and DMCA + H_2O + CO_2 mixtures, respectively. As can be seen from Fig. 17, CO_2-loaded solutions of MCA exhibit a three-phase region where an aqueous liquid phase, poor in CO_2, and an organic liquid phase, rich in amine and CO_2, coexist with a vapour phase. Phase diagrams at T = 313.15, 333.15, and 363.15 K are presented in the figure. The impact of changes in temperature on the

Table 10
Measured solubility of CO_2 in aqueous DMCA solutions. Θ_{CO_2} corresponds to the CO_2 loading, defined as the number of moles of CO_2 absorbed in the corresponding liquid phase per mole of amine in that phase. The upper phase is denoted as U and the lower as L. The * indicates that the final amine content is expressed on a water basis.

T/K	P_{CO_2}/kPa	Phase equilibria	Θ_{CO_2}	Final amine content* w_{amine}%
313.15	12.7	VLLE (U)	0.015 ± 0.002	85.3 ± 1.3
		VLLE (L)	0.911 ± 0.048	17.0 ± 0.5
313.15	19.0	VLLE (U)	0.017 ± 0.003	92.9 ± 1.4
		VLLE (L)	0.955 ± 0.050	21.3 ± 1.1
313.15	33.8	VLE	0.865 ± 0.045	26.8 ± 0.6
313.15	50.7	VLE	0.958 ± 0.054	26.7 ± 0.9
333.15	9.7	VLLE (U)	0.013 ± 0.002	93.7 ± 1.1
		VLLE (L)	0.917 ± 0.047	6.6 ± 0.7
333.15	13.9	VLLE (U)	0.014 ± 0.004	93.6 ± 1.1
		VLLE (L)	1.039 ± 0.052	7.7 ± 0.4
333.15	22.0	VLLE (U)	0.017 ± 0.004	94.5 ± 1.1
		VLLE (L)	1.101 ± 0.056	9.1 ± 0.3
333.15	48.6	VLLE (U)	0.018 ± 0.003	94.8 ± 1.6
		VLLE (L)	1.047 ± 0.055	14.0 ± 0.5
333.15	70.9	VLLE (U)	0.019 ± 0.003	95.3 ± 1.1
		VLLE (L)	0.935 ± 0.049	19.6 ± 1.8
363.15	10.1	VLLE (U)	0.014 ± 0.003	96.4 ± 1.2
		VLLE (L)	1.177 ± 0.071	2.8 ± 0.3
363.15	20.3	VLLE (U)	0.014 ± 0.004	96.8 ± 0.6
		VLLE (L)	1.181 ± 0.063	2.7 ± 0.2
363.15	30.4	VLLE (U)	0.019 ± 0.003	97.0 ± 1.8
		VLLE (L)	1.237 ± 0.069	3.5 ± 0.2
363.15	40.5	VLLE (U)	0.017 ± 0.003	97.0 ± 1.1
		VLLE (L)	1.219 ± 0.061	4.2 ± 0.2
363.15	68.6	VLLE (U)	0.017 ± 0.004	97.0 ± 1.6
		VLLE (L)	0.894 ± 0.050	4.9 ± 0.6

phase behaviour of the mixture is remarkable; at higher temperatures a much-reduced three-phase region is found.

Predicted ternary phase diagrams for the DMCA + H_2O + CO_2 mixture at $T = 333.15$ K and several pressures corresponding to the experimental partial pressures of CO_2 reported in Table 10 are presented in Fig. 18. Regions of vapour–liquid–liquid coexistence are also seen. As the pressure is increased, the extent of the three-phase region is seen to grow, mostly driven by the enhanced phase separation of the H_2O + CO_2 mixture at the conditions considered.

5. Conclusions

We have developed thermodynamically-consistent group-contribution models for use within the SAFT-γ Mie approach that relate the molecular structure and fluid-phase equilibria of several chemical families of amines to the performance of aqueous solutions of these compounds for CO_2 absorption. We have complemented existing literature data on relevant mixtures with new data for the phase equilibria of two phase-change solvents in aqueous mixtures with CO_2.

Our description of the mixtures is based on intermolecular potential models that incorporate association sites to mediate the formation of aggregates representing the key species in the chemical reactions of CO_2 with amine-based solvents. Through our extensive studies of several mixtures, this has been shown to enable accurate predictions of the available speciation experimental data without the need to define reaction equilibrium constants explicitly. The proposed modelling approach has been found to deliver reliable calculations and predictions of the CO_2 solubility, chemical speciation, fluid-phase behaviour, and mixing properties of aqueous solutions of carbon dioxide and alkylpolyamines, alkanolamines and cyclohexylamines, including the prediction of regions of vapour–liquid–liquid equilibria for varying conditions of CO_2 loading, pressure, and temperature.

In the current work 19 new SAFT-γ Mie group interactions have been developed. To capture the effect of hydroxyl groups on the interactions between amine groups and water in aqueous solutions of short alkanolamines, second-order group parameters have been introduced. These second-order group parameters have also been shown to provide an accurate description of the solubility of CO_2 in aqueous solutions of short-chain primary, secondary, and ternary alkanolamines. The models have been used to predict the concentration of ionic species in mixtures of MEA and DEA with water and CO_2. A remarkable level of accuracy has been achieved considering that no speciation has been used in parameter estimation and that ionic species are modelled implicitly.

The transferability of the proposed parameters to other mixtures of amines, H_2O and CO_2 and other conditions not used for the parameter estimation has also been demonstrated with predictions of fluid-phase equilibria and heat of absorption. Good agreement with experimental data has been observed across a wide range of systems. This will allow one to assess the fluid-phase behaviour of candidate solvents (alkylpolyamines, alkanolamines, and cyclohexylamines) based on knowledge of their molecular structure only. Similarly, blends of these compounds can be assessed predictively with this approach for future use in solvent design studies. Our current work thus represents a useful predictive platform to guide the search for optimal solvent candidates in the context of CO_2 capture. It has the potential to achieve a substantial reduction in the experimental effort and time required to screen and identify promising candidates from an absorption perspective. It can also readily be integrated into computer-aided solvent design methods that allow one totake a much wider set of metrics into consideration to assess solvent suitability, including safety, health and environmental performance, as well as cost and energy consumption [122]. This is especially important in view of the varying hazards that are associated with individual solvents and the impacts that may result from solvent losses and the formation of degradation products.

CRediT authorship contribution statement

Felipe A. Perdomo: Methodology, Equilibrium modeling and prediction, Software, Writing – original draft, Analysis of results. **Siti H. Khalit:** Methodology, Equilibrium modeling and prediction, Software. **Edward J. Graham:** Methodology, Equilibrium modeling and prediction, Software, Analysis of results. **Fragkiskos Tzirakis:** Equilibrium experiments and CO_2 solubility measurements, Analysis of results. **Athanasios I. Papadopoulos:** Writing – original draft, Review & editing, Visualization, Funding acquisition, Project administration. **Ioannis Tsivintzelis:** Equilibrium experiments and CO_2 solubility

measurements, Analysis of results, Review & editing. **Panos Seferlis:** Review & editing, Project administration, Funding acquisition. **Claire S. Adjiman:** Conceptualization, Writing – review & editing, Supervision, Project administration, Funding acquisition. **George Jackson:** Conceptualization, Writing – review & editing, Supervision. **Amparo Galindo:** Conceptualization, Writing – original draft review & editing, Supervision.

Declaration of competing interest

The authors declare that they have no known competing financial interests or personal relationships that could have appeared to influence the work reported in this paper.

Acknowledgements

Felipe A. Perdomo, Amparo Galindo, George Jackson, Claire S. Adjiman, Fragkiskos Tzirakis, Ioannis Tsivintzelis, Athanasios I. Papadopoulos, Panos Seferlis thank the European Union's Horizon 2020 research and innovation program (Grant 727503 - ROLINCAP – H2020-LCE-2016-2017/H2020-LCE-2016-RES-CCS-RIA) for financial support. Siti H. Khalit thanks PETRONAS Research for funding a Ph.D. studentship. We also gratefully acknowledge support from the Engineering and Physical Sciences Research Council (EPSRC) of the UK (Grants EP/E016340, EP/J014958, and EP/P006965) to the Molecular Systems Engineering group. Claire S. Adjiman is thankful to EPSRC, United Kingdom for the award of a Leadership Fellowship (Grant EP/J003840) and Amparo Galindo is thankful to the Royal Academy of Engineering, United Kingdom and Lilly for support of a Research Chair (Grant RCSRF18193).

Data statement

Data underlying this article can be accessed on Zenodo at https://doi.org/10.5281/zenodo.7291414, and used under the Creative Commons Attribution license.

Appendix A. Combining rules

The unlike segment diameter σ_{kl} for groups k and l is always obtained using the Lorentz arithmetic mean of the like diameters [123]:

$$\sigma_{kl} = \frac{\sigma_{kk} + \sigma_{ll}}{2}. \tag{A.1}$$

The unlike dispersion energy ϵ_{kl} between groups k and l is obtained by applying an augmented geometric mean (Berthelot-like rule), which also accounts for asymmetries in size [124]:

$$\epsilon_{kl} = \frac{\sqrt{\sigma_{kk}^3 \sigma_{ll}^3}}{\sigma_{kl}^3} \sqrt{\epsilon_{kk}\epsilon_{ll}}. \tag{A.2}$$

The exponents of the unlike segment-segment interaction λ_{kl}^r and λ_{kl}^a are obtained as

$$\lambda_{kl} = 3 + \sqrt{(\lambda_{kk} - 3)(\lambda_{ll} - 3)}, \tag{A.3}$$

which results from the imposition of the geometric mean of the integrated van der Waals energy (Berthelot rule) for a Sutherland fluid of range λ_{kl} [84]. The bonding volume $K_{kl,ab}$ and association energy parameter $\epsilon_{kl,ab}^{HB}$ between unlike sites a and b ($a \neq b$) on groups k and l, respectively, can also be approximated following arithmetic and geometric averages as

$$K_{kl,ab} = \left(\frac{\sqrt[3]{K_{kk,ab}} + \sqrt[3]{K_{ll,ab}}}{2} \right)^3, \tag{A.4}$$

and

$$\epsilon_{kl,ab}^{HB} = \left(\epsilon_{kk,ab}^{HB} \, \epsilon_{ll,ab}^{HB} \right)^{\frac{1}{2}}. \tag{A.5}$$

For two sites of the same type, the interaction is usually set to zero:

$$K_{kl,aa} = 0, \tag{A.6}$$

and

$$\epsilon_{kl,aa}^{HB} = 0. \tag{A.7}$$

These combining rules provide a good first estimate of the values of the required unlike group parameters; however, it is best to use experimental data when available to estimate these parameters, especially in the case of the unlike dispersion energies.

Appendix B. Group-based representation of compounds and mixtures

Table B.1
SAFT-γ Mie group contribution representation of the systems studied in the current work. The systems are listed in the first column, and the corresponding groups used to represent them are listed in the second column following the numbering given in Table 2. The first-order unlike interactions used are given the third column using the format "group 1–group 2". Their specific values can be found in Tables 4 and 5. Second-order unlike interactions are listed in the final column, with values given in Tables 6 and 7.

Compound/Mixture	Groups	First-order interactions	Second-order interactions
MPZ	1, 4, 5, 6	1–4, 1–5, 1–6, 4–5, 4–6, 5–6	NA
MPZ + H_2O + CO_2	1, 4, 5, 6, 12, 14	1–12, 1–14, 4–12, 4–14, 5–12, 5–14, 6–12, 6–14, 12–14	NA
EPZ	1, 3, 4, 5, 6	1–3, 1–4, 1–5, 1–6, 3–4, 3–5, 3–6, 4–5, 4–6, 5–6	NA
EPZ + H_2O + CO_2	1, 3, 4, 5, 6, 12, 14	1–12, 1–14,3–12, 3–14, 4–12, 4–14, 5–12, 5–14, 6–12, 6–14, 12–14	NA
PZ	1, 5	1–5	NA
PZ + H_2O + CO_2	1, 5, 12, 14	1–5, 1–12, 1–14, 5–12, 5–14, 12–14	NA
MAPA	3, 4, 8, 9	3–4, 3–8, 3–9, 4–8, 4–9, 8–9	NA
MAPA + H_2O + CO_2	3, 4, 8, 9, 12, 14	3–12, 3–14, 4–12, 4–14, 8–12, 8–14, 9–12, 9–14, 12–14	NA
DETA	3, 8, 9	3–8, 3 –9, 8–9	NA
DETA + H_2O + CO_2	3, 8, 9, 12, 14	3–12, 3–14, 8–12, 8–14, 9–12, 9–14, 12–14	NA
MEA	9, 3, 13	9–3, 9–13, 3–13	NA
MEA + H_2O + CO_2	9, 3, 13, 12, 14	3–12, 3–14, 13–14	9–12, 9–14, 12–13, 12–14
MPA	9, 3, 13	9–3, 9–13, 3–13	NA
MPA + H_2O + CO_2	9, 3, 13, 12, 14	3–12, 3–14, 13–14	9–12, 9–14, 12–13, 12–14
MDEA	3, 4, 7, 13	3–4, 3–7, 3–13, 4–7, 4–13, 7–13	NA
MDEA + H_2O + CO_2	3, 4, 7, 13, 12, 14	3–12, 3–14, 4–12, 4–14, 12–14, 13–14	7–12, 7–14, 12–13
DMMEA	3, 4, 7, 13	3–4, 3–7, 3–13, 4–7, 4–13, 7–13	NA
DMMEA + H_2O + CO_2	3, 4, 7, 13, 12, 14	3–12, 3–14, 4–12, 4–14, 12–14, 13–14	7–12, 7–14, 12–13
DEA	3, 8, 13	3–8, 3–13, 8–13	NA
DEA + H_2O + CO_2	3, 8, 13, 12, 14	3–12, 3–14, 12–14, 13–14	8–12, 8–14, 12–13
MCA	1, 4, 10	1–4, 1–10, 4–10	NA
MCA + H_2O + CO_2	1, 4, 10, 12, 14	1–12, 1–14, 4–12, 4–14, 10–12, 10–14, 12–14	NA
DMCA	1, 4, 11	1–4, 1–11, 4–11	NA
DMCA + H_2O + CO_2	1, 4, 11, 12, 14	1–12, 1–14, 4–12, 4–14, 12–14	NA

Appendix C. Workflow for characterization of SAFT-γ Mie solvent groups

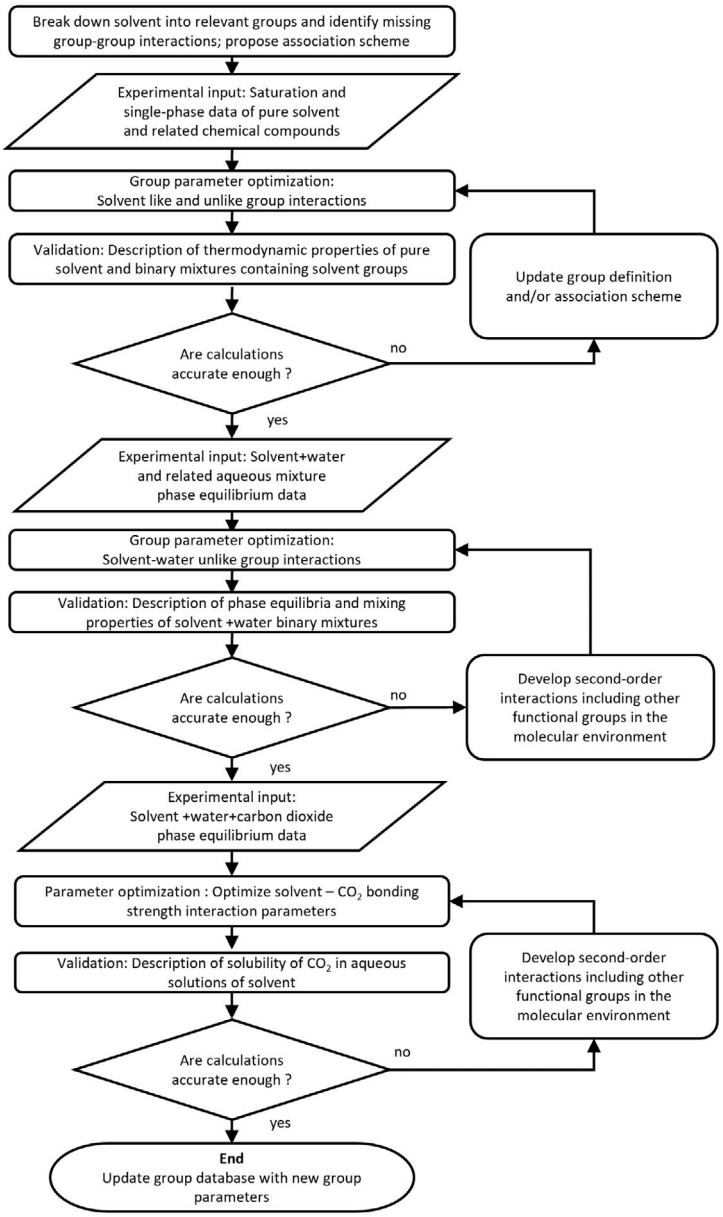

Appendix D. Pure alkanol amine properties

The experimental data for the saturation and single-phase properties of the primary and secondary alkanolamine solvents considered in our work are compared to the SAFT-γ calculations and predictions in Fig. D.19 and the corresponding comparison for tertiary amines are presented in Fig. D.20.

As can be seen from Fig. D.19 a good description of the vapour–liquid equilibria in terms of the vapour pressure and saturated-liquid density is obtained in the case of pure primary and secondary alkanolamines, specifically MEA, MPA, and DEA. In order to model these amines, the NH_2–CH_2OH, NH–CH_2OH interaction parameters are determined in the current work. The saturation properties of MDEA and DMMEA are given in Fig. D.20, together with a comparison of the single-phase isobaric heat capacity of DMMEA. The N–CH_2OH interaction needed to model these two amines is determined including available data of MDEA, but no data for DMMEA is used in the parameter estimation procedure. The calculations presented here for this solvent are fully predictive.

In the SAFT-γ Mie approach a heteronuclear model is implemented, which means that pure compound data alone, mixture data only, or pure and mixture data of related systems can be considered simultaneously in estimating group parameters. For example, some of the group interactions used here to model the pure amines are determined by examining different families (e.g., the CH_2–CH_3 interaction is determined based on data for the *n*-alkanes only). In modelling aqueous mixtures of amines, mixture data is required, as water is a molecular group, but often the data used relates to different mixtures altogether (e.g., data for aqueous mixtures of alkylamines are used to determine the NH_2–H_2O interactions). These interactions can then be transferred and used in a fully predictive fashion to model the systems of interest (on the proviso that they contain the same groups).

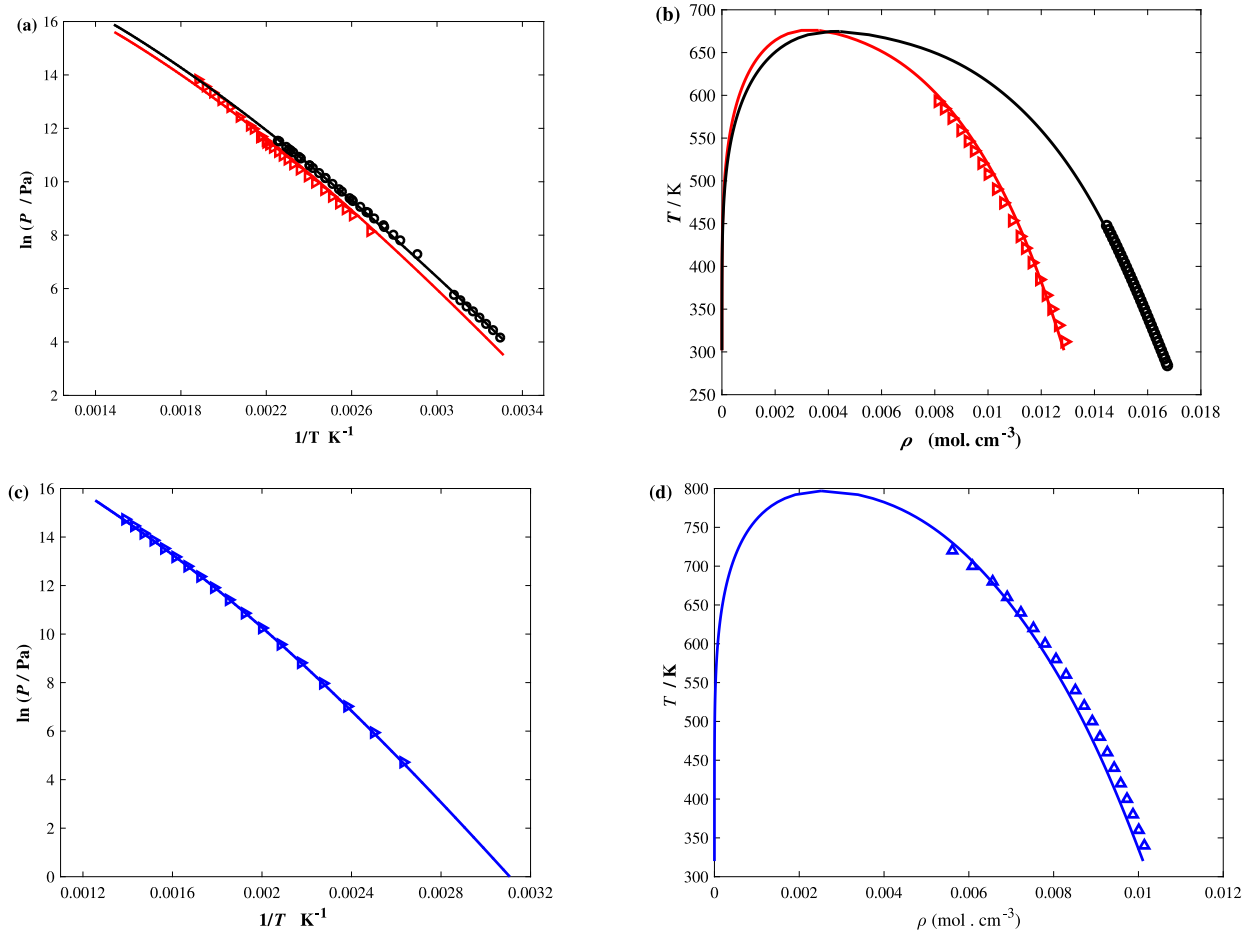

Fig. D.19. Vapour pressure P (Clausius–Clapeyron representation) ((a) and (c)) and vapour–liquid coexistence densities ρ as a function of temperature T ((b) and(d)) for pure alkanolamines. The symbols correspond to the experimental data (black circles for MEA [109,110], red triangles for MPA [112], and blue triangles for DEA [114]), and the continuous curves to the corresponding SAFT-γ Mie calculations.

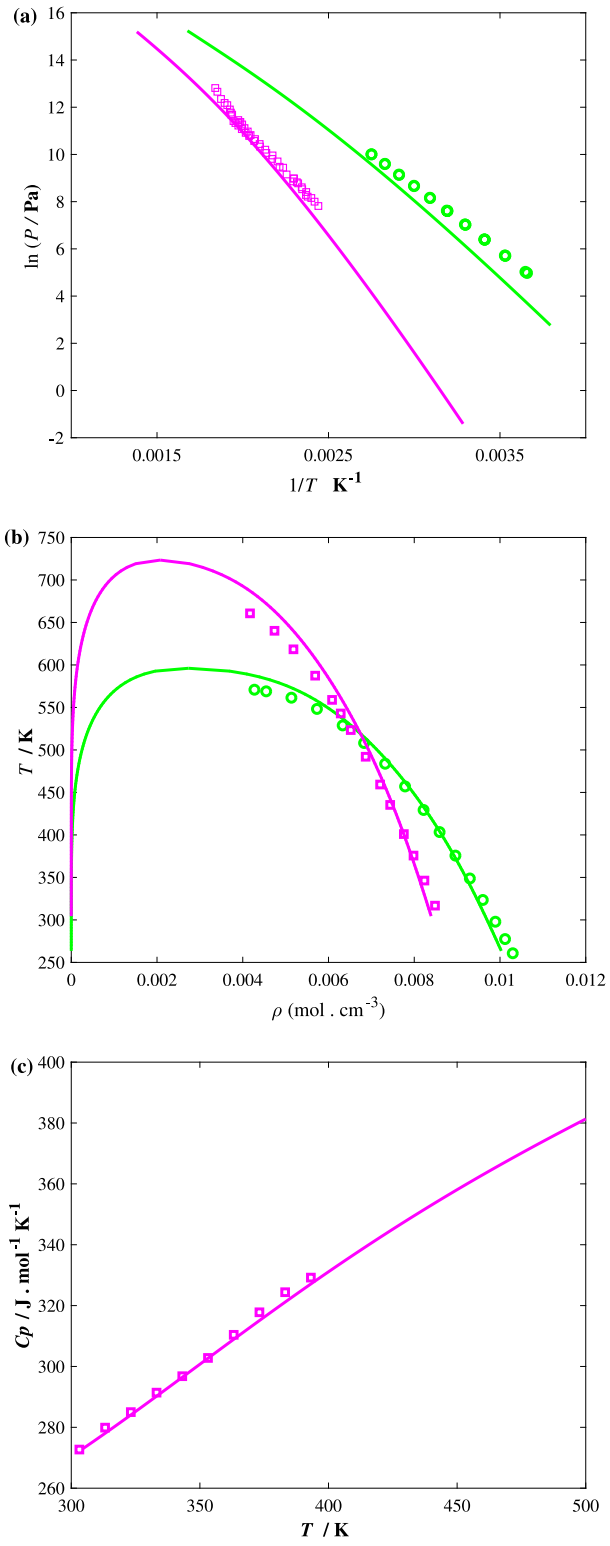

Fig. D.20. (a) Vapour pressure P (Clausius–Clapeyron representation), (b) coexisting vapour–liquid densities ρ as a function of temperature T, and (c) isobaric (P = 1.01 bar) liquid heat capacity of pure tertiary alkanolamines. The symbols correspond to experimental data (magenta squares [115–117] for MDEA, and green circles [56] for DMMEA). The continuous curves correspond to SAFT-γ Mie calculations.

References

[1] N. MacDowell, N. Florin, A. Buchard, J. Hallett, A. Galindo, G. Jackson, C.S. Adjiman, C.K. Williams, N. Shah, P. Fennell, An overview of CO_2 capture technologies, Energy Environ. Sci. 3 (11) (2010) 1645–1669.

[2] F. Tzirakis, I. Tsivintzelis, A.I. Papadopoulos, P. Seferlis, Experimental measurement and assessment of equilibrium behaviour for phase change solvents used in CO_2 capture, Chem. Eng. Sci. 199 (2019) 20–27.

[3] G.-I. Kaminishi, C. Yokoyama, T. Shinji, Vapor pressures of binary mixtures of carbon dioxide with benzene, n-hexane and cyclohexane up to 7 MPa, Fluid Phase Equilib. 34 (1) (1987) 83–99.

[4] R744-CO_2 saturation properties (temperature table 2) - (updated 7/26/08), 2022, URL www.ohio.edu/mechanical/thermo/property_tables/CO2/CO2_TempSat2.html.

[5] S. Vitu, J.-N. Jaubert, J. Pauly, J.-L. Daridon, D. Barth, Phase equilibria measurements of CO_2 + methyl cyclopentane and CO_2 + isopropyl cyclohexane binary mixtures at elevated pressures, J. Supercrit. Fluids 44 (2) (2008) 155–163.

[6] D. Robinson, C.-J. Chen, H.-J. Ng, The Equilibrium Phase Properties of Selected Naphthenic Binary Systems: Ethylcyclohexane-Carbon Dioxide, Ethylcyclohexane-Nitrogen, Ethylcyclohexane-Methane, Gas Processors Association, 1981.

[7] A.F. Ciftja, A. Hartono, H.F. Svendsen, Experimental study on phase change solvents in CO_2 capture by NMR spectroscopy, Chem. Eng. Sci. 102 (2013) 378–386.

[8] V. Ermatchkov, Á. Pérez-Salado Kamps, D. Speyer, G. Maurer, Solubility of carbon dioxide in aqueous solutions of piperazine in the low gas loading region, J. Chem. Eng. Data 51 (5) (2006) 1788–1796.

[9] H. Li, Y. Le Moullec, J. Lu, J. Chen, J.C.V. Marcos, G. Chen, F. Chopin, CO_2 solubility measurement and thermodynamic modeling for 1-methylpiperazine/water/CO_2, Fluid Phase Equilib. 394 (2015) 118–128.

[10] H. Li, Y. Le Moullec, J. Lu, J. Chen, J.C.V. Marcos, G. Chen, Solubility and energy analysis for CO_2 absorption in piperazine derivatives and their mixtures, Int. J. Greenh. Gas Control 31 (2014) 25–32.

[11] M.W. Arshad, H.F. Svendsen, P.L. Fosbøl, N. von Solms, K. Thomsen, Equilibrium total pressure and CO_2 solubility in binary and ternary aqueous solutions of 2-(diethylamino) ethanol (DEEA) and 3-(methylamino) propylamine (MAPA), J. Chem. Eng. Data 59 (3) (2014) 764–774.

[12] Q. Ye, X. Wang, Y. Lu, Experimental investigation and thermodynamic modeling of phase transition and equilibria in a biphasic solvent system for CO_2 capture, Ind. Eng. Chem. Res. 57 (29) (2018) 9627–9640.

[13] M.W. Arshad, P.L. Fosbøl, N. von Solms, H.F. Svendsen, K. Thomsen, Heat of absorption of CO_2 in phase change solvents: 2-(diethylamino) ethanol and 3-(methylamino) propylamine, J. Chem. Eng. Data 58 (7) (2013) 1974–1988.

[14] A. Belabbaci, A. Razzouk, I. Mokbel, J. Jose, L. Negadi, Isothermal vapor- liquid equilibria of (monoethanolamine+ water) and (4-methylmorpholine+ water) binary systems at several temperatures, J. Chem. Eng. Data 54 (8) (2009) 2312–2316.

[15] S.-B. Park, H. Lee, Vapor-liquid equilibria for the binary monoethanolamine+ water and monoethanolamine+ ethanol systems, Korean J. Chem. Eng. 14 (2) (1997) 146–148.

[16] A. Nath, E. Bender, Isothermal vapor-liquid equilibriums of binary and ternary mixtures containing alcohol, alkanolamine, and water with a new static device, J. Chem. Eng. Data 28 (4) (1983) 370–375.

[17] W. Wilding, L. Wilson, G. Wilson, Vapor-liquid equilibrium measurements on eight binary mixtures, Am. Inst. Chem (1) (1991) 6–23.

[18] S. Horstmann, P. Mougin, F. Lecomte, K. Fischer, J. Gmehling, Phase equilibrium and excess enthalpy data for the system methanol+ 2, 2 '-diethanolamine+ water, J. Chem. Eng. Data 47 (6) (2002) 1496–1501.

[19] M. Abedinzadegan Abdi, A. Meisen, A novel process for diethanolamine recovery from partially degraded solutions. 1. Process description and phase equilibria of the DEA- BHEP- THEED- hexadecane system, Ind. Eng. Chem. Res. 38 (8) (1999) 3096–3104.

[20] Z. Cai, R. Xie, Z. Wu, Binary isobaric vapor- liquid equilibria of ethanolamines+ water, J. Chem. Eng. Data 41 (5) (1996) 1101–1103.

[21] R.E. Dugas, G.T. Rochelle, CO_2 absorption rate into concentrated aqueous monoethanolamine and piperazine, J. Chem. Eng. Data 56 (5) (2011) 2187–2195.

[22] A.V. Rayer, Y. Armugam, A. Henni, P. Tontiwachwuthikul, High-pressure solubility of carbon dioxide (CO_2) in aqueous 1-methyl piperazine solution, J. Chem. Eng. Data 59 (11) (2014) 3610–3623.

[23] A. Hartono, M. Saeed, A.F. Ciftja, H.F. Svendsen, Binary and ternary VLE of the 2-amino-2-methyl-1-propanol (AMP)/piperazine (Pz)/water system, Chem. Eng. Sci. 91 (2013) 151–161.

[24] T. Nguyen, M. Hilliard, G.T. Rochelle, Amine volatility in CO_2 capture, Int. J. Greenh. Gas Control 4 (5) (2010) 707–715.

[25] A. Kossmann, S. Rehfeldt, P. Moser, H. Klein, Process study for stripping components in absorption–desorption processes for CO_2-removal from power plant flue gases, Chem. Eng. Res. Des. 99 (2015) 236–247.

[26] J. Zhang, R. Misch, Y. Tan, D.W. Agar, Novel thermomorphic biphasic amine solvents for CO_2 absorption and low-temperature extractive regeneration, Chem. Eng. Technol. 34 (9) (2011) 1481–1489.

[27] F. Liu, M. Fang, W. Dong, T. Wang, Z. Xia, Q. Wang, Z. Luo, Carbon dioxide absorption in aqueous alkanolamine blends for biphasic solvents screening and evaluation, Appl. Energy 233 (2019) 468–477.

[28] S. Zhang, Y. Shen, L. Wang, J. Chen, Y. Lu, Phase change solvents for post-combustion CO_2 capture: Principle, advances, and challenges, Appl. Energy 239 (2019) 876–897.

[29] D.D. Pinto, S.A. Zaidy, A. Hartono, H.F. Svendsen, Evaluation of a phase change solvent for CO_2 capture: Absorption and desorption tests, Int. J. Greenh. Gas Control 28 (2014) 318–327.

[30] D.D. Pinto, H. Knuutila, G. Fytianos, G. Haugen, T. Mejdell, H.F. Svendsen, CO_2 post combustion capture with a phase change solvent. Pilot plant campaign, Int. J. Greenh. Gas Control 31 (2014) 153–164.

[31] J. Zhang, Y. Qiao, W. Wang, R. Misch, K. Hussain, D.W. Agar, Development of an energy-efficient CO_2 capture process using thermomorphic biphasic solvents, Energy Procedia 37 (2013) 1254–1261.

[32] A. Idrissi, P. Jedlovszky, Thermodynamics of mixing primary alkanolamines with water, J. Phys. Chem. B 122 (23) (2018) 6251–6259.

[33] A.J. Lopes Jesus, J.S. Redinha, Molecular insight into the amine–water interaction: A combined vibrational, energetic and NBO/NEDA study, Comput. Theoret. Chem. 1023 (2013) 74–82.

[34] R.M. Stephenson, Mutual solubility of water and aliphatic amines, J. Chem. Eng. Data 38 (4) (1993) 625–629.

[35] E.F. Da Silva, H.F. Svendsen, Computational chemistry study of reactions, equilibrium and kinetics of chemical CO_2 absorption, Int. J. Greenh. Gas Control 1 (2) (2007) 151–157.

[36] S.S. Laddha, P.V. Danckwerts, Reaction of CO_2 with ethanolamines: kinetics from gas-absorption, Chem. Eng. Sci. 36 (3) (1981) 479–482.

[37] P.D. Vaidya, V.V. Mahajani, Kinetics of the reaction of CO_2 with aqueous formulated solution containing monoethanolamine, N-methyl-2-pyrrolidone, and diethylene glycol, Ind. Eng. Chem. Res. 44 (6) (2005) 1868–1873.

[38] N. McCann, D. Phan, X. Wang, W. Conway, R. Burns, M. Attalla, G. Puxty, M. Maeder, Kinetics and mechanism of carbamate formation from CO_2 (aq), carbonate species, and monoethanolamine in aqueous solution, J. Phys. Chem. A 113 (17) (2009) 5022–5029.

[39] G. Maurer, Phase equilibria in chemical reactive fluid mixtures, Fluid Phase Equilib. 116 (1–2) (1996) 39–51.

[40] F. Bougie, M.C. Iliuta, CO_2 absorption in aqueous piperazine solutions: experimental study and modeling, J. Chem. Eng. Data 56 (4) (2011) 1547–1554.

[41] N. Sadegh, E.H. Stenby, K. Thomsen, Thermodynamic modeling of CO_2 absorption in aqueous N-Methyldiethanolamine using Extended UNIQUAC model, Fuel 144 (2015) 295–306.

[42] E.T. Hessen, T. Haug-Warberg, H.F. Svendsen, The refined e-NRTL model applied to CO_2–H_2O–alkanolamine systems, Chem. Eng. Sci. 65 (11) (2010) 3638–3648.

[43] T.J. Edwards, G. Maurer, J. Newman, J.M. Prausnitz, Vapor-liquid equilibria in multicomponent aqueous solutions of volatile weak electrolytes, AIChE J. 24 (6) (1978) 966–976.

[44] Á.P.-S. Kamps, J. Xia, G. Maurer, Solubility of CO_2 in (H_2O+ piperazine) and in (H_2O + MDEA + piperazine), AIChE J. 49 (10) (2003) 2662–2670.

[45] W. Böttinger, M. Maiwald, H. Hasse, Online NMR spectroscopic study of species distribution in MEA–H_2O–CO_2 and DEA–H2O–CO_2, Fluid Phase Equilib. 263 (2) (2008) 131–143.

[46] W. Böttinger, M. Maiwald, H. Hasse, Online NMR spectroscopic study of species distribution in MDEA- H2O- CO_2 and MDEA- PIP- H2O- CO_2, Ind. Eng. Chem. Res. 47 (20) (2008) 7917–7926.

[47] K. Thomsen, Modeling electrolyte solutions with the extended universal quasichemical (UNIQUAC) model, Pure Appl. Chem. 77 (3) (2005) 531–542.

[48] M.W. Arshad, P.L. Fosbøl, N. von Solms, K. Thomsen, CO_2 capture with liquid-liquid phase change solvents: a thermodynamic study, Energy Procedia 114 (2017) 1671–1681.

[49] M.W. Arshad, N. von Solms, K. Thomsen, Thermodynamic modeling of liquid–liquid phase change solvents for CO_2 capture, Int. J. Greenh. Gas Control 53 (2016) 401–424.

[50] G. Bollas, C.-C. Chen, P. Barton, Refined electrolyte-NRTL model: Activity coefficient expressions for application to multi-electrolyte systems, AIChE J. 54 (6) (2008) 1608–1624.

[51] M. Born, Volumen und hydratationswärme der ionen, Z. Phys. 1 (1) (1920) 45–48.

[52] A.A. Rashin, B. Honig, Reevaluation of the Born model of ion hydration, J. Phys. Chem. 89 (26) (1985) 5588–5593.

[53] C. Dell'Era, P. Uusi-Kyyny, E.-L. Rautama, M. Pakkanen, V. Alopaeus, Thermodynamics of aqueous solutions of methyldiethanolamine and diisopropanolamine, Fluid Phase Equilib. 299 (1) (2010) 51–59.

[54] I. Kim, H.F. Svendsen, E. Børresen, Ebulliometric determination of vapor-liquid equilibria for pure water, monoethanolamine, n-methyldiethanolamine, 3-(methylamino)-propylamine, and their binary and ternary solutions, J. Chem. Eng. Data 53 (11) (2008) 2521–2531.

[55] A. Soames, A. Al Helal, S. Iglauer, A. Barifcani, R. Gubner, Experimental vapor–liquid equilibrium data for binary mixtures of methyldiethanolamine in water and ethylene glycol under vacuum, J. Chem. Eng. Data 63 (5) (2018) 1752–1760.

[56] N. Chiali-Baba-Ahmed, F. Dergal, L. Negadi, I. Mokbel, Measurement and correlation of the (vapor+ liquid) equilibria of pure 4-ethylmorpholine, 1, 2-dimethylisopropylamine and N, N-dimethylethanolamine, and their binary aqueous solutions, J. Chem. Thermodyn. 63 (2013) 44–51.

[57] Y. Maham, A.E. Mather, L.G. Hepler, Excess molar enthalpies of (water+ alkanolamine) systems and some thermodynamic calculations, J. Chem. Eng. Data 42 (5) (1997) 988–992.

[58] M. Mundhwa, A. Henni, Molar excess enthalpy (HmE) for various {alkanolamine (1)+ water (2)} systems at T=(298.15, 313.15, and 323.15) K, J. Chem. Thermodyn. 39 (11) (2007) 1439–1451.

[59] C. Secuianu, V. Feroiu, D. Geană, Phase behavior for carbon dioxide+ ethanol system: Experimental measurements and modeling with a cubic equation of state, J. Supercrit. Fluids 47 (2) (2008) 109–116.

[60] C. Secuianu, V. Feroiu, D. Geana, High-pressure phase equilibria for the carbon dioxide+ 1-propanol system, J. Chem. Eng. Data 53 (10) (2008) 2444–2448.

[61] W. Fürst, H. Renon, Representation of excess properties of electrolyte solutions using a new equation of state, AIChE J. 39 (2) (1993) 335–343.

[62] G. Vallée, P. Mougin, S. Jullian, W. Fürst, Representation of CO_2 and H_2S absorption by aqueous solutions of diethanolamine using an electrolyte equation of state, Ind. Eng. Chem. Res. 38 (9) (1999) 3473–3480.

[63] L. Chunxi, W. Fürst, Representation of CO_2 and H_2S solubility in aqueous MDEA solutions using an electrolyte equation of state, Chem. Eng. Sci. 55 (15) (2000) 2975–2988.

[64] P.W.J. Derks, H. Dijkstra, J. Hogendoorn, G.F. Versteeg, Solubility of carbon dioxide in aqueous piperazine solutions, AIChE J. 51 (8) (2005) 2311–2327.

[65] F.-Y. Jou, A.E. Mather, F.D. Otto, The solubility of CO_2 in a 30 mass percent monoethanolamine solution, Can. J. Chem. Eng. 73 (1) (1995) 140–147.

[66] D. Lal, F.D. Otto, A.E. Mather, The solubility of H_2S and CO_2 in a diethanolamine solution at low partial pressures, Can. J. Chem. Eng. 63 (4) (1985) 681–685.

[67] J.P. Jakobsen, J. Krane, H.F. Svendsen, Liquid-phase composition determination in CO_2 - H_2O- alkanolamine systems: An NMR study, Ind. Eng. Chem. Res. 44 (26) (2005) 9894–9903.

[68] K. Leontiadis, E. Tzimpilis, D. Aslanidou, I. Tsivintzelis, Solubility of CO_2 in 3-amino-1-propanol and in N-methyldiethanolamine aqueous solutions: Experimental investigation and correlation using the CPA equation of state, Fluid Phase Equilib. 500 (2019) 112254.

[69] F.-Y. Jou, J.J. Carroll, A.E. Mather, F.D. Otto, The solubility of carbon dioxide and hydrogen sulfide in a 35 wt% aqueous solution of methyldiethanolamine, Can. J. Chem. Eng. 71 (2) (1993) 264–268.

[70] C. Tong, C.C. Perez, J. Chen, J.-C.V. Marcos, T. Neveux, Y. Le Moullec, Measurement and calculation for CO_2 solubility and kinetic rate in aqueous solutions of two tertiary amines, Energy Procedia 37 (2013) 2084–2093.

[71] W.G. Chapman, G. Jackson, K.E. Gubbins, Phase equilibria of associating fluids: chain molecules with multiple bonding sites, Mol. Phys. 65 (5) (1988) 1057–1079.

[72] W.G. Chapman, K.E. Gubbins, G. Jackson, M. Radosz, SAFT: Equation-of-state solution model for associating fluids, Fluid Phase Equilib. 52 (1989) 31–38.

[73] G. Jackson, W.G. Chapman, K.E. Gubbins, Phase equilibria of associating fluids: Spherical molecules with multiple bonding sites, Mol. Phys. 65 (1) (1988) 1–31.

[74] I.G. Economou, M.D. Donohue, Chemical, quasi-chemical and perturbation theories for associating fluids, AIChE J. 37 (12) (1991) 1875–1894.

[75] R.A. Heidemann, J. Prausnitz, A van der waals-type equation of state for fluids with associating molecules, Proc. Natl. Acad. Sci. 73 (6) (1976) 1773–1776.

[76] Y.H. Tan, Study of CO_2-Absorption into Thermomorphic Lipophilic Amine Solvents (Ph.D. thesis), 2010.

[77] N. Mac Dowell, F. Llovell, C.S. Adjiman, G. Jackson, A. Galindo, Modeling the fluid phase behavior of carbon dioxide in aqueous solutions of monoethanolamine using transferable parameters with the SAFT-VR approach, Ind. Eng. Chem. Res. 49 (4) (2010) 1883–1899.

[78] J. Rodriguez, N. Mac Dowell, F. Llovell, C.S. Adjiman, G. Jackson, A. Galindo, Modelling the fluid phase behaviour of aqueous mixtures of multifunctional alkanolamines and carbon dioxide using transferable parameters with the SAFT-VR approach, Mol. Phys. 110 (11–12) (2012) 1325–1348.

[79] A. Chremos, E. Forte, V. Papaioannou, A. Galindo, G. Jackson, C.S. Adjiman, Modelling the phase and chemical equilibria of aqueous solutions of alkanolamines and carbon dioxide using the SAFT-γ SW group contribution approach, Fluid Phase Equilib. 407 (2016) 280–297.

[80] A. Gil-Villegas, A. Galindo, P.J. Whitehead, S.J. Mills, G. Jackson, A.N. Burgess, Statistical associating fluid theory for chain molecules with attractive potentials of variable range, J. Chem. Phys. 106 (1997) 4168–4186.

[81] A. Galindo, L. Davies, A. Gil-Villegas, G. Jackson, The thermodynamics of mixtures and the corresponding mixing rules in the SAFT-VR approach for potentials of variable range, Mol. Phys. 93 (2) (1998) 241–252.

[82] A. Lymperiadis, C.S. Adjiman, A. Galindo, G. Jackson, A group contribution method for associating chain molecules based on the statistical associating fluid theory (SAFT-γ), J. Chem. Phys. 127 (23) (2007) 234903.

[83] A. Lymperiadis, C.S. Adjiman, G. Jackson, A. Galindo, A generalisation of the SAFT-γ group contribution method for groups comprising multiple spherical segments, Fluid Phase Equilib. 274 (1–2) (2008) 85–104.

[84] V. Papaioannou, T. Lafitte, C. Avendano, C.S. Adjiman, G. Jackson, E.A. Müller, A. Galindo, Group contribution methodology based on the statistical associating fluid theory for heteronuclear molecules formed from Mie segments, J. Chem. Phys. 140 (5) (2014) 054107.

[85] S. Dufal, T. Lafitte, A.J. Haslam, A. Galindo, G.N. Clark, C. Vega, G. Jackson, The A in SAFT: developing the contribution of association to the Helmholtz free energy within a Wertheim TPT1 treatment of generic Mie fluids, Mol. Phys. 113 (9–10) (2015) 948–984.

[86] G. Jackson, S. Dufal, T. Lafitte, A. Haslam, A. Galindo, G. Clark, C. Vega, Corrigendum: The A in SAFT: developing the contribution of association to the Helmholtz free energy within a Wertheim TPT1 treatment of generic Mie fluids, Mol. Phys. 116 (10) (2018) 283–285.

[87] F.A. Perdomo, S.H. Khalit, C.S. Adjiman, A. Galindo, G. Jackson, Description of the thermodynamic properties and fluid-phase behavior of aqueous solutions of linear, branched, and cyclic amines, AIChE J. 67 (3) (2021) e17194.

[88] S. Dufal, V. Papaioannou, M. Sadeqzadeh, T. Pogiatzis, A. Chremos, C.S. Adjiman, G. Jackson, A. Galindo, Prediction of thermodynamic properties and phase behavior of fluids and mixtures with the SAFT-γ Mie group-contribution equation of state, J. Chem. Eng. Data 59 (2014) 3272–3288.

[89] M.S. Wertheim, Fluids with highly directional attractive forces. I. Statistical thermodynamics, J. Stat. Phys. 35 (1) (1984) 19–34.

[90] M.S. Wertheim, Fluids with highly directional attractive forces. II. Thermodynamic perturbation theory and integral equations, J. Stat. Phys. 35 (1) (1984) 35–47.

[91] M.S. Wertheim, Fluids with highly directional attractive forces. III. Multiple attraction sites, J. Stat. Phys. 42 (3) (1986) 459–476.

[92] M.S. Wertheim, Fluids with highly directional attractive forces. IV. Equilibrium polymerization, J. Stat. Phys. 42 (3) (1986) 477–492.

[93] J.M. Prausnitz, R.N. Lichtenthaler, E.G. De Azevedo, Molecular Thermodynamics of Fluid-Phase Equilibria, Pearson Education, 1998.

[94] L.L. Lee, Molecular Thermodynamics of Nonideal Fluids, Butterworth-Heinemann, 2016.

[95] F.E. Pereira, G. Jackson, A. Galindo, C.S. Adjiman, The HELD algorithm for multicomponent, multiphase equilibrium calculations with generic equations of state, Comput. Chem. Eng. 36 (2012) 99–118.

[96] F.E. Pereira, G. Jackson, A. Galindo, C.S. Adjiman, A duality-based optimisation approach for the reliable solution of (P, T) phase equilibrium in volume-composition space, Fluid Phase Equilib. 299 (1) (2010) 1–23.

[97] gPROMS v. 3.4.0, PSE Ltd., London, 2011, http:www.psenterprise.com.

[98] Siemens PSE, Using gPROMS's state-of-the-art parameter estimation facilities, 2022, URL https://www.psenterprise.com/products/gproms/technologies/model-validation. (Accessed 03 March 2022).

[99] V. Papaioannou, F. Calado, T. Lafitte, S. Dufal, M. Sadeqzadeh, G. Jackson, C.S. Adjiman, A. Galindo, Application of the SAFT-γ Mie group contribution equation of state to fluids of relevance to the oil and gas industry, Fluid Phase Equilib. 416 (2016) 104–119.

[100] A.J. Haslam, A. González-Pérez, S. Di Lecce, S.H. Khalit, F.A. Perdomo, S. Kournopoulos, M. Kohns, T. Lindeboom, M. Wehbe, S. Febra, et al., Expanding the applications of the SAFT-γ mie group-contribution equation of state: prediction of thermodynamic properties and phase behavior of mixtures, J. Chem. Eng. Data (2020).

[101] P. Hutacharoen, S. Dufal, V. Papaioannou, R.M. Shanker, C.S. Adjiman, G. Jackson, A. Galindo, Predicting the solvation of organic compounds in aqueous environments: from alkanes and alcohols to pharmaceuticals, Ind. Eng. Chem. Res. 56 (38) (2017) 10856–10876.

[102] I.I. Alkhatib, L.M. Pereira, A. AlHajaj, L.F. Vega, Performance of non-aqueous amine hybrid solvents mixtures for CO_2 capture: A study using a molecular-based model, J. CO2 Util. 35 (2020) 126–144.

[103] C. Cleeton, O. Kvam, R. Rea, L. Sarkisov, M.G. De Angelis, Competitive H_2S–CO_2absorption in reactive aqueous methyldiethanolamine solution: Prediction with ePC-SAFT, Fluid Phase Equilib. 511 (2020) 112453.

[104] L.M. Pereira, F. Llovell, L.F. Vega, Thermodynamic characterisation of aqueous alkanolamine and amine solutions for acid gas processing by transferable molecular models, Appl. Energy 222 (2018) 687–703.

[105] A. Hartono, E.F. da Silva, H.F. Svendsen, Kinetics of carbon dioxide absorption in aqueous solution of diethylenetriamine (DETA), Chem. Eng. Sci. 64 (14) (2009) 3205–3213.

[106] A. Sherwood, J.M. Prausnitz, The heat of solution of gases at high pressure, AIChE J. 8 (4) (1962) 519–521.

[107] S. Di Lecce, G. Lazarou, S.H. Khalit, C.S. Adjiman, G. Jackson, A. Galindo, L. McQueen, Modelling and prediction of the thermophysical properties of aqueous mixtures of choline geranate and geranic acid (CAGE) using SAFT-γ Mie, RSC Adv. 9 (65) (2019) 38017–38031.

[108] S. Di Lecce, G. Lazarou, S.H. Khalit, D. Pugh, C.S. Adjiman, G. Jackson, A. Galindo, L. McQueen, Correction: Modelling and prediction of the thermophysical properties of aqueous mixtures of choline geranate and geranic acid (CAGE) using SAFT-γ Mie, RSC Adv. 10 (33) (2020) 19463–19465.

[109] S. Kapteina, K. Slowik, S.P. Verevkin, A. Heintz, Vapor pressures and vaporization enthalpies of a series of ethanolamines, J. Chem. Eng. Data 50 (2) (2005) 398–402.

[110] A. Valtz, C. Coquelet, D. Richon, Volumetric properties of the monoethanolamine–methanol mixture at atmospheric pressure from 283.15 to 353.15 K, Thermochim. Acta 428 (1–2) (2005) 185–191.

[111] A.V. Rayer, A. Henni, P. Tontiwachwuthikul, Molar heat capacities of solvents used in CO_2 capture: A group additivity and molecular connectivity analysis, Can. J. Chem. Eng. 90 (2) (2012) 367–376.

[112] K. Klepácová, P.J. Huttenhuis, P.W. Derks, G.F. Versteeg, Vapor pressures of several commercially used alkanolamines, J. Chem. Eng. Data 56 (5) (2011) 2242–2248.

[113] L. Hepler, A. Mather, A. Hakin, R. Marriott, et al., Molar heat capacities of alkanolamines from 299.1 to 397.8 K group additivity and molecular connectivity analyses, J. Chem. Soc. Faraday Trans. 93 (9) (1997) 1747–1750.

[114] P. Linstrom, Nist standard reference database number 69, NIST Chem. WebBook (2003).

[115] T. Daubert, G. Hutchison, Vapor pressure of 18 pure industrial chemicals, in: AIChE Symp. Ser, Vol. 86, No. 279, 1990, pp. 93–114.

[116] A.V. Rayer, A. Henni, P. Tontiwachwuthikul, Molar heat capacities of solvents used inCO_2 capture: A group additivity and molecular connectivity analysis, Can. J. Chem. Eng. 90 (2) (2012) 367–376.

[117] B. Hawrylak, S.E. Burke, R. Palepu, Partial molar and excess volumes and adiabatic compressibilities of binary mixtures of ethanolamines with water, J. Solut. Chem. 29 (6) (2000) 575–594.

[118] D.H. Lam, A. Jangkamolkulchai, K.D. Luks, Liquid—liquid—vapor phase equilibrium behavior of certain binary carbon dioxide+ n-alkanol mixtures, Fluid Phase Equilib. 60 (1–2) (1990) 131–141.

[119] C.V. Brand, E. Graham, J. Rodríguez, A. Galindo, G. Jackson, C.S. Adjiman, On the use of molecular-based thermodynamic models to assess the performance of solvents for CO_2 capture processes: monoethanolamine solutions, Faraday Discuss. 192 (2016) 337–390.

[120] D.K. Eriksen, G. Lazarou, A. Galindo, G. Jackson, C.S. Adjiman, A.J. Haslam, Development of intermolecular potential models for electrolyte solutions using an electrolyte SAFT-VR Mie equation of state, Mol. Phys. 114 (18) (2016) 2724–2749.

[121] M. Kohns, G. Lazarou, S. Kournopoulos, E. Forte, F.A. Perdomo, G. Jackson, C.S. Adjiman, A. Galindo, Predictive models for the phase behaviour and solution properties of weak electrolytes: nitric, sulphuric, and carbonic acids, Phys. Chem. Chem. Phys. 22 (27) (2020) 15248–15269.

[122] A.I. Papadopoulos, F.A. Perdomo, F. Tzirakis, G. Shavalieva, I. Tsivintzelis, P. Kazepidis, E. Nessi, S. Papadokonstantakis, P. Seferlis, A. Galindo, G. Jackson, C.S. Adjiman, Molecular engineering of sustainable phase-change solvents: From digital design to scaling-up for CO_2 capture, Chem. Eng. J. 420 (2021) 127624.

[123] J.S. Rowlinson, F. Swinton, The thermodynamics of liquid mixtures, in: Liquids and Liquid Mixtures, third ed., Butterworth-Heinemann, London, 1982, pp. 86–131, (Chapter 4).

[124] A.J. Haslam, A. Galindo, G. Jackson, Prediction of binary intermolecular potential parameters for use in modelling fluid mixtures, Fluid Phase Equilib. 266 (1–2) (2008) 105–128.